GROUND-BASED THERMAL OBSERVATIONS OF TWO LAVA LAKES AT MOUNT EREBUS VOLCANO, ANTARCTICA IN DECEMBER 2004

JULIE ANN CALKINS

Independent Study

Submitted in Partial Fulfilment
of the requirements for the Degree of
Masters of Science in Geochemistry

Department of Earth and Environmental Science
New Mexico Institute of Mining and Technology

Socorro, New Mexico

May 2006

TABLE OF CONTENTS

	Page
TITLE PAGE	1
TABLE OF CONTENTS	2
LIST OF FIGURES	4
LIST OF TABLES	6
ABSTRACT	7
LIST OF SYMBOLS	8
1. Introduction	9
2. Mount Erebus Volcano	11
2.1 Field Description	11
2.2 Historical Activity of Erebus Volcano	13
2.3 Volcanic Activity in 2004	14
3. Methods	16
3.1 Thermal Camera Instrument Specifications	16
3.2 Recording Conditions	16
4. Results	18
4.1 Lava Lake Surface Temperatures	18
4.1.1 Errors and Corrections to Surface Temperatures	20
4.2 Radiative Heat Output	22
4.2.1 Main Lake	22
4.2.2 Werner's Lava Lake	25
5. Discussion	27
5.1 Total Lava Lake Heat and Mass Flux	27
5.1.1 Lava Lake Heat Flux	27

5.1.2 Mass Flux 28

5.1.3 Previous Thermal Output Determinations 30

5.1.4 Previous Mass Flux Determinations 32

5.1.5 Comparison to Erta Ale Lava Lake 32

5.2 Visual Observations and Interpretation 33

5.2.1 Main Lava Lake 33

5.2.2 Werner's Lava Lake 35

5.3 Volcanological Implications 37

5.3.1 Magma and Lava Lake System 37

5.3.2 Mass Balance Models 41

6. Conclusions 44

Appendix A. Infrared Radiometry and Thermography 45

Appendix B. Thermal Camera Instrument Specifications 49

Appendix C. Determination of Lava Lake Areas 51

Appendix D. Image Recording and Data Processing 56

Appendix E. Convective Heat Flux Calculation 59

Appendix F. Lava Lake Surface Temperature Corrections 62

Acknowledgements 64

References 65

CD: Thermal Imagery Data Spreadsheets CD

LIST OF FIGURES

		Page
Figure 1	Two photos taken in December 2004 from the north-western Main Crater rim of the lava lakes in the Inner Crater of Mount Erebus volcano. The views are looking southeast. The photos are stitched together to show their relative positions. a. Main Lava Lake b. Werner's Lava Lake, Lakes are ~50 meters apart on the Inner Crater floor.	10
Figure 2	Location of Mount Erebus Volcano, Ross Island, Antarctica, with Main and Side Craters shown.	12
Figure 3	Main Crater of Erebus Volcano. Main lava lake surface area is ~1400 m^2 and Werner's lava lake is ~1200 m^2. The Side Crater is seen to the west of the Main Crater.	12
Figure 4	a) Thermal image of Main lava lake with a gas bubble. b) Histogram of pixel temperature distribution from FLIR image. Temperatures are uncorrected and gridlines are increments of 10% of the total number of lava lake pixels.	18
Figure 5	Graph portraying the average daily maximum and daily mean lava lake surface temperatures for the Main Lake (ML) and Werner's Lake (WL). Error bars are $\pm$ one standard deviation.	19
Figure 6	Graph shows corrected surface temperatures. The dashed line corresponds to a 1:1 relationship between observed and corrected temperatures. Gas absorption corrections show a 30-70°C underestimate in observed temperatures.	21
Figure 7	Plot of radiative power output calculated for the Main lava lake. Saturated pixels have been added to values indicated by black arrows (as explained above). Measurements every 10 seconds.	23
Figure 8	a) Sudden changes in the radiative heat output due to gas interference and the bursting of a Strombolian bubble on the surface of the lava lake. b) Thermal image of bubble bursting on the surface of the Main lava lake. c) Sequence of images showing a puff of gas affectively cooling the measured lava lake surface temperature as it moves from the left of the image across to exit the frame on the right.	24
Figure 9	Radiative output of Werner's lava lake calculated from 10 second images. Sudden drops in Q_{rad} are attributed to gas absorption.	25
Figure 10	Radiative heat variations of Werner's lava lake due to dynamism of lava convection and influx, not to gas absorption or bubbles. Arrows indicate gaps in record from instrument shutting itself off.	26
Figure 11	The upwelling source of Main Lava Lake (dashed oval) is the site of the highest surface temperatures. Arrows show general flow pattern and dashed line indicates area of plate build-up.	34
Figure 12	Schematic diagram of Main Lava Lake system in a) plan view showing vectors of surface motion and b) cross-sectional view showing inferred convection cycle.	35
Figure 13	Three locations of upwelling are shown as dashed circles for the two that are visible and a question mark for the flow of lava that is	36

	assumed to be hidden by a rock outcrop. a) 12 Dec 2004, cooled area is indicated by a dashed line near the northern source. b) 21 Dec 2004	
Figure 14	Schematic diagram of Werner's Lava Lake in a) plan view showing vectors of surface motion and sites of upwelling and b) cross-sectional view showing inferred convection cycle.	36
Figure 15	21 Dec 2004 Aerial thermal image of both lava lakes: Main Lake on the left and Werner's Lake on the right.	37
Figure 16	Cartoon of convection driven by degassing in a bi-flow conduit with discrete gas bubbles.	38
Figure 17	a) Lava lake model with bi-flow conduits connecting magma reservoir to Main Lake (ML), Active Vent (AV), and Werner's Lake (WL). b) Lava lake model with Main Lake as the exposed top of the magma reservoir, and conduits linking Active Vent and Werner's Lake to the magmatic system.	40

LIST OF TABLES

		Page
Table 1	Summary of Erebus Volcano activity, 1972-present	13
Table 2	Summary of Lava Lake thermal outputs determined in this study.	28
Table 3	Lava lake mass flux as affected by varying Δf and ΔT. Main Lava Lake (above) and Werner's Lava Lake (below).	30
Table 4	Summary of results of previous thermal studies on Erebus volcanic activity.	31
Table 5	Summary and comparison of ground-based thermal results on Erta 'Ale lava lake.	33

Abstract

Mount Erebus, a large intraplate stratovolcano dominating the western side of Ross Island, Antarctica, hosts the world's only phonolite lava lakes. Volcanic activity at Mt. Erebus in December 2004 was characterized by the presence of two convecting lava lakes within the Inner Crater. The long-lived Main Lake, ~1400 m^2 in area, had up to 10 small strombolian eruptions daily. A new ~1200-1000 m^2 lake formed at Werners fumarole in December with lava flowing from a source in the Inner Crater floor. The radiative heat flux from the 2 lakes was measured in the 2004/05 Antarctic field season using a compact thermal infrared imaging camera. Daily thermal IR imagery surveys from the Main Crater rim have improved our understanding of the volcanic system by enabling identification of upwelling and downwelling sites and detailed mapping of the lava lake surface temperatures. Thermal observations also present high temporal resolution images of lava lake convection patterns and strombolian activity. The radiative heat output calculated for the Main Lake and Werner's Lake were 34-37 MW and 20-24 MW, respectively. Mass flux needed to sustain this heat loss is estimated as 90-200 kg/s. These results are used to evaluate the minimum volume of the magmatic reservoir and the conduit radius of the Mt. Erebus volcanic system.

LIST OF SYMBOLS

Parameter	Description	Units/Value
Δf	Crystallized mass fraction	0.3-0.5
ΔT	Temperature difference from magmatic to degassed lava	K
A	Area	m^2
c_{gas}	Specific heat capacity of gas	1600 J/kg*K
C_L	Latent heat of crystallization	3×10^5 J/kg
c_p	Heat capacity of the magma	1150 J/kg*K
D	Diameter	m^2
$E_{\lambda b}$	Spectral radiative power of a blackbody	W-$\mu m^4/m^2$
E_b	Radiative power of a blackbody	w/m2
E_r	Radiative power of a real object	w/m2
F_{gas}	Total gas flux	0.86 kg/s
F_{H20}	Total water flux	9.4 kg/s
g	Acceleration of gravity	9.8 $m\,s^{-2}$
k	Thermal conductivity	W m^{-1} K^{-1}
L	Length	m
L_v	Latent heat of condensation	2.26×10^6 J/kg
Pr	Prandtl number	0.68
Q_{conv}	Convective heat flux	MW
Q_{gas}	Gas heat flux	MW
Q_{rad}	Radiative heat flux	MW
Q_{tot}	Total heat flux	MW
r	Radius of the lava lale	m
Ra_L	Rayleigh number	
T	Temperature	K
T_∞	Temperature at free-stream conditions	K
T_f	"Film" temperature	K
T_s	Temperature of surface	K
β	Temperature coefficient of thermal conductivity	K^{-1}
ϵ	Emissivity	1.0
λ	Wavelength	um
ν	Velocity	$m^2\ s^{-1}$
σ	Stefan-Boltzmann constant	5.67×10^{-8} W/m^2

1. Introduction

Lava lakes are rare and fascinating phenomena that exist at only a few volcanoes in the world. Active lava lakes are fed by volatile-rich, hot, buoyant magma rising via a conduit from a deeper, larger reservoir or magma chamber. Inactive lava lakes, or lava pools, form by the ponding of lava flows and are not connected to a magma chamber (Swanson, 1972). Inactive lava lakes, such as Kilauea Iki, have proved very useful in studies of cooling and crystallization (Evans and Moore, 1968; Hardee, 1980; Jellinek and Kerr, 2001), however they provide limited insights into conduit dynamics and underlying magmatic processes (Swanson, 1979). Active lava lakes are considered to be the exposed top of a convecting magma column, and as such, provide a window into the underlying magmatic system (Tilling, 1987; Tazieff, 1994) . Convection within an active lava lake, and between the lake and the underlying magma reservoir, is likely driven and sustained by density gradients created by crystallization, degassing, and cooling (Worster et al., 1993; Kazahaya et al., 1994; Jaupart and Tait, 1995; Stevenson and Blake, 1998). Long-lived persistently-active lava lakes are especially rare and occur at only three volcanoes: Nyiragongo, Democratic Republic of Congo, Erta 'Ale, Ethiopia, and Mount Erebus, Ross Island, Antarctica (Tazieff, 1994; Harris et al., 1999a).

In this study thermal observations of Mt. Erebus volcano are interpreted to probe the magmatic processes responsible for permanent lava lake activity. I report the results of ground-based thermal radiometric imaging surveys of the lava lakes of Erebus volcano. Using the lava lake surface temperatures, I derive the total heat flux from the lava lakes and the equivalent magma mass flux necessary to sustain the thermal output. I also compare measured lava temperatures with those inferred from earlier petrologic calculations, a single optical pyrometer temperature measurement

(Kyle, 1977; McClelland et al., 1989; Dunbar et al., 1994), and observations made using satellite remote sensing techniques (Glaze et al., 1989; Rothery and Oppenheimer, 1994; Harris et al., 1997; Harris et al., 1999a; Harris et al., 1999b; Wright et al., 2002; Wright and Flynn, 2004; Davies et al., 2005, submitted). The results of the new observations, comprised of more accurate determinations of lava lake surface temperature and power output, are explored in the light of conceptual and physical models for magma convection in conduits in order to shed further light on the volcano-magmatic system of Mount Erebus Volcano.

In December 2004, two active anorthoclase phonolite lava lakes were present in the Inner Crater of Mount Erebus Volcano: I refer to these as the Main lava lake, which has been active since at least 1972, and Werner's lava lake, which became an active lava lake in December 2004 and was a glowing and sputtering hornito in previous years (Fig.1) (Kyle, *pers comm.*). Both lakes were actively circulating and overturning, thereby providing a unique opportunity for surficial observation of thermal activity and convection driven by less apparent magmatic processes.

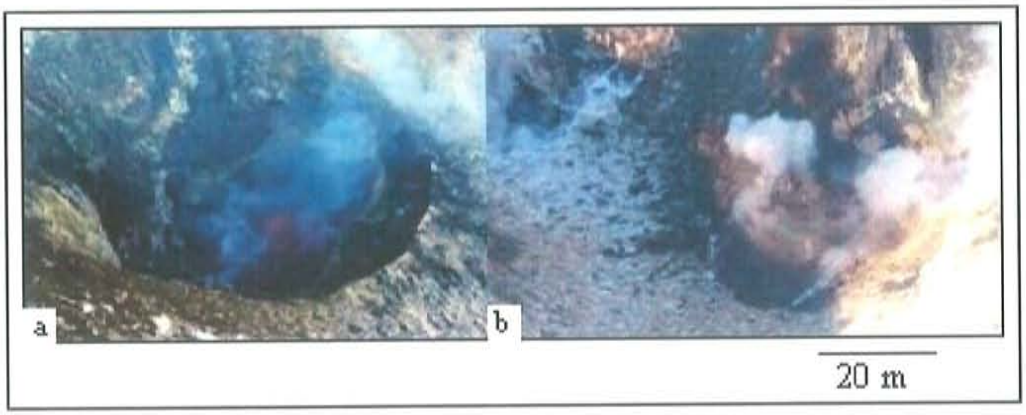

Figure 1 Two photos taken in December 2004 from the north-western Main Crater rim of the lava lakes in the Inner Crater of Mount Erebus volcano. The views are looking southeast. The photos are stitched together to show their relative positions. a. Main Lava Lake b. Werner's Lava Lake, Lakes are ~50 meters apart on the Inner Crater floor.

2. Mount Erebus Volcano

2.1 Erebus volcano

Mount Erebus volcano (77°32'S, 176°10'E, 3794 m) is an alkaline intraplate volcano formed as a result of crustal thinning, recent faulting, and magmatic activity along a section of the regionally-extensive West Antarctic Rift System, known as the Terror Rift (Kyle, 1990b; Kyle, 1990a; LeMasurier, 1990; Behrendt et al., 1991). The Terror Rift, is also associated with geothermally-active Mount Melbourne Volcano, ~400 km north of Ross Island (Behrendt et al., 1991)

Mt. Erebus is a large polygenetic stratovolcano which dominates the western side of Ross Island. It is surrounded by the extinct volcanoes Mts. Terra Nova and Terror to the east, and Mt Bird to the north (Fig. 1). Mount Erebus has a complex morphology resulting from more than 1.3 Myr of eruptive activity (Esser *et al.*, 2004). Remnants of extrusive events preceding the current activity are evident morphologically as lava flows (pahoehoe), lava tubes, truncated cones, escarpments, and exposed ridges. All historical activity has occurred within the current summit cone, which hosts the Main and Side Craters (600 m and 300 m diameter, respectively). The summit cone is surrounded by a flat 4 km-wide plateau at ~3000 m asl, which has been interpreted by Moore and Kyle (1987) to be a prior collapsed caldera, later filled with lava flows and pyroclastic material.

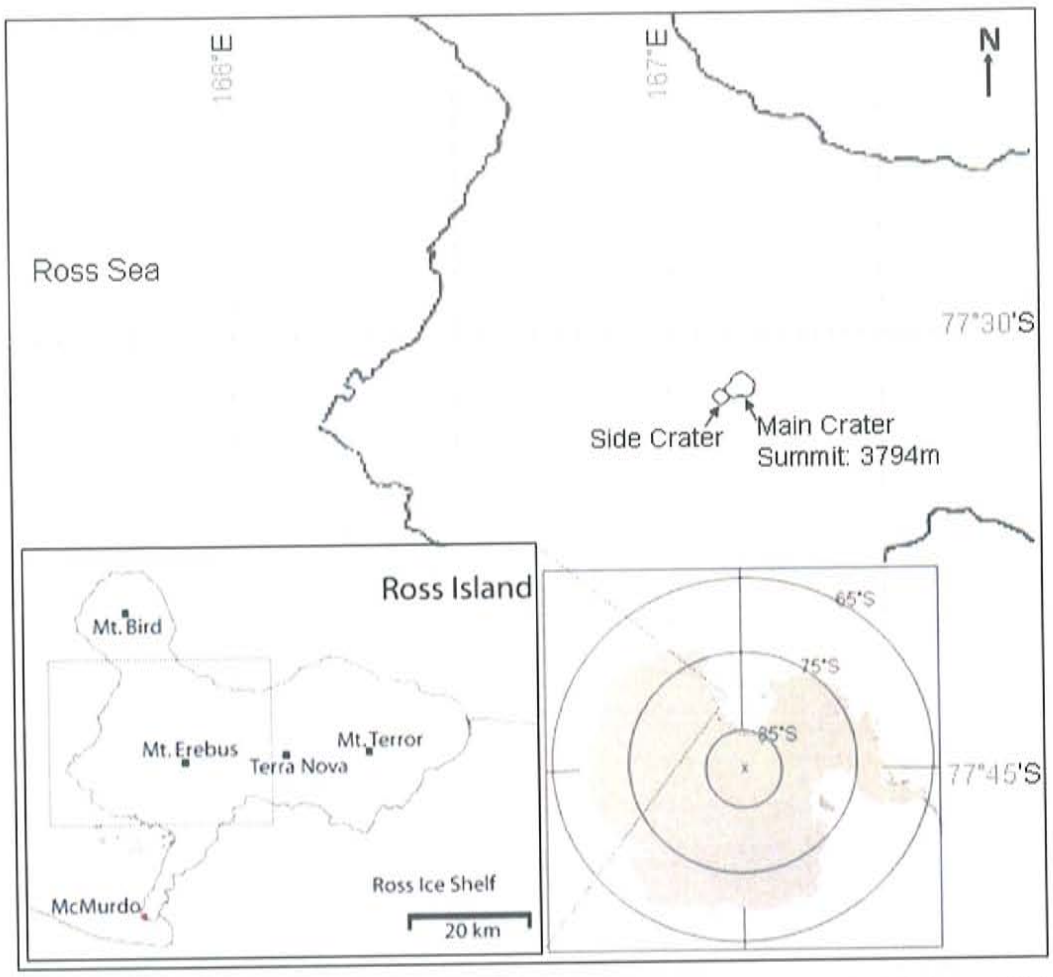

Figure 2. Location of Mount Erebus Volcano, Ross Island, Antarctica, with Main and Side Craters shown.

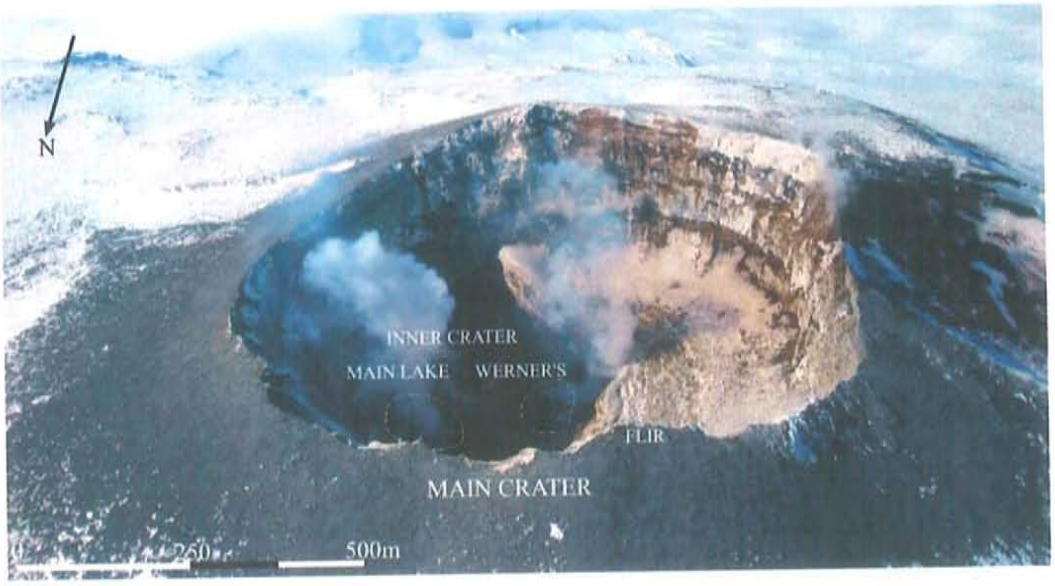

Figure 3. Main Crater of Erebus Volcano. Main lava lake surface area is ~1400 m^2 and Werner's lava lake is ~1200 m^2. The Side Crater is seen to the west of the Main Crater.

2.2 Historical activity of Erebus Volcano

Mount Erebus Volcano was discovered and named by Rear Admiral Sir James Clarke Ross on 28 January 1841 (Ross, 1847; Ross, 1982). Robert McCormick, surgeon on the HMS Erebus, described the scene as "a stupendous volcanic mountain in a high state of activity" (Ross, 1982). In 1908 David et al., (1909) reported a thick smoky cloud emanating from the volcano, lit from below with an eerie red glow. This was observed from their camp at Cape Royds, some 15-20 km away from Erebus. Giggenbach *et al.* (1973) were the first to record a "partly frozen lava lake" in the summit cone of Mount Erebus, a feature that has been present in varying dimensions and character ever since.

The activity at Erebus is characterised by its convecting, degassing lava lake (Main lava lake), which has a radius of 10-30 m. It exhibits phases of frequent Strombolian eruptions such as began in 2005 (see Table 1). Detailed scientific observations from 1972 to present describe periods of explosive activity, the largest of which occurred in September 1984 and erupted 1×10^6 m^3 of phonolite lava and ash (Caldwell and Kyle, 1994). The activity of peripheral vents and fumaroles has not been recorded routinely, save the long-standing activity of two hornitos/fumaroles, named the Ash Vent and Werner's Vent.

Table 1. Summary of Erebus Volcano activity, 1972-present

Observation Period	Description of Activity	Reference
1972-1973	Strong fumarolic activity observed, though the view of the Main Crater floor was obscured.	(Giggenbach *et al.*, 1973)
1972-1976	Lava lake expands to semicircle ~60m diameter.	(Kyle, 1986)
Jan 1978	One to six eruptions from the Active Vent per day. Bubbles and incandescence observed at the site of upwelling in lava lake.	(Kyle and McIntosh, 1978)
Dec 1978	Two lava flows seen: 1) Lava flow from the main lava lake	(Kyle, 1979)

	2) Lava flow from a fumarole/hornito in the southwest part of the Inner Crater.*	
1979	A 60m x 45m lava lake present with two upwelling sites.	(Kyle et al 1982)
Sept 1984 –Jan 1985	Increase in activity. Large bombs, up to 10 m diameter, are launched 600m over the Main Crater rim, landing up to 1.2 km down the flank. Eruptions heard at McMurdo Station, 25km away. Lava lake is buried.	(Kyle, 1986)
1985-1999	Explosive activity was decreased in magnitude and frequency, likely related to exhumation of the lava lake and resultant free gas emissions. Main lava lake persisted in various sizes and orientations, with occasional lava flows from fumaroles.	(Kyle, 1986; Dibble et al., 1994)
4 Sept 1990	Lava flow from lava lake	(Dibble, in prep)
Oct.1993	Two large phreatic eruptions occurred forming a new crater about 30m across in the western edge of the Main Crater floor.	(Dibble et al., 1994)
Aug 1999-Nov 2002	Increased seismic activity and Strombolian eruptions, small lava flow from Werner's Vent	(Ruiz, 2003)
Nov 2002-2004	Eruptive activity ceased	(Ruiz, 2003)
Dec 2004 –Jan 2005	The Main lava lake persists with an area of ~1400m^2. Werner's lava lake formed on 12th Dec 2004. Up to 10 small eruptions occur per day.	(This study)
Nov 2005 –Jan 2006	Period of heightened activity with large eruptions occurring in Main Lake 0-6 times daily, with bombs over the Main Crater Rim. Also daily eruptions at small hornito, Active Vent. Lava lake activity ceased at Werner's Lake with resumed hornito presence.	(This study)

*This hornito was later named after Dr. Werner F. Giggenbach (Werner's Vent/Lake).

2.3 Volcanic activity in 2004

In December 2004 there were two convecting anorthoclase phonolite lava lakes with occasional (0-10 daily) small Strombolian eruptions (Jones, *pers. comm.)*, feeding a constant plume of gas and aerosol (Fig. 3). The Main lava lake was persistently convecting and degassing albeit with a slight decrease in surface area from the previous year. The second lake appeared at Werner's Vent (unofficial name

following use by (Aster et al., 2003) during the annual field campaign on or about 12 December 2004. The vent, located ~60-70 m from the south-western margin of the Main lava lake has been present since the 1970's (Kyle *et al.*, 1982). The vent was the site of short lava flows in 1979 (Kyle, 1979) and 2002 (Kyle, *pers. comm.*) and an incandescent glow has frequently been observed inside Werner's Vent since December 1974 (Kyle et al., 1982). Werner's lava lake grew in size to ~1200 m^2, clearly fed by a flow of lava near its southern edge. By 22 December 2004, the last day of thermal observation, the north-eastern part of the lake had cooled and solidified, reducing the actively convecting surface area of the lake to ~1000 m^2.

From the crater rim, the surface of the Main Lake appears below the lip of a shallow pit crater. The surface of the lake is dark and puckered with cracks and fissures exposing incandescent lava. Eruptions eject spatter onto the sides of the pit crater wall and up the side of the inner crater wall. The surface of Werner's Lake is also dark except at the sub-aerial site of material flow into the lake, where material is red-orange until joining the principal lake body. Werner's Lake extended to the north until a levee was formed by a cooled lobe of lava.

3. Methods

3.1 Thermal Camera Specifications

Thermal measurements were made in 2004 using an Agema Thermovision 550 IR camera. This instrument is a stirling-cooled focal-plane array infrared radiometer camera sensitive to emitted radiation in the 3.6-5.0 μm window producing calibrated thermal images with +/- 2°C accuracy (details in Appendix B). All images have dimensions of 320 x 240 pixels, collected at a path length of ~300 m, which, given the 1.1 mrad instantaneous field of view of the instrument, resulted in a ground resolution cell (pixel size) of ~0.4 m x 0.4 m on the lava lake surface. The camera was calibrated with an internal temperature reference and could be adjusted to one of three temperature ranges dependent on the target's temperature. Infrared measurements were mostly collected with the mid-range temperature setting (200-850°C). Two datasets were also recorded using the high-range setting (600-1500°C), and from these data the best determination of the lava temperature were derived. Note that no single temperature range captured the whole spectrum of surface temperatures of the lake.

3.2 Field Observations

In 2004 the thermal camera was mounted on a tripod and the lava lakes were observed from Shackleton's Cairn on the Main Crater ~300 m line of sight from the surface of the Main lava lake (Fig. 2). This location was chosen because it was logistically straightforward to reach and allowed excellent views of both lava lakes. Two visible video cameras and an FTIR gas spectrometer were also operated from this location.

Thermal infrared measurements and visual observations were typically recorded between midday and 7 pm local time from 10 to 24 December 2004. Over 10,000 images were collected. Infrared images were recorded continuously with time steps of between 1 and 10 s. Recording was unfortunately interrupted every 15-60 min due to a camera or software fault, possibly due to the cold air temperatures. The camera was covered in bubble-wrap designed to insulate it from the cold, and shield it from the wind, ash, and snow. Weather conditions during recording were comparatively mild, with an air temperature of 0 to -20°C and wind below 10 knots.

Laser range-finding binoculars were used to determine that the path length from the observation site on the crater rim to the Main lava lake's surface was ~300 m. The area of the Main lava lake was estimated as ~1400 m^2. Werner's Lake was ~ 1200 m^2 in area on 12 December 2004 and, after considerable cooling along the margins, was ~1000 m^2 by 20 December 2004 (see details in Appendix C).

4. Results

4.1 Lava Lake Surface Temperatures

Corrected temperatures of the lava lake surfaces ranged between 275°C and 974°C for Main Lake, and 275°C and 1006°C for Werner's lava lake (Fig. 4). Observed temperatures varied depending on the vigour of circulation and overturning in the lake. At any one time, particular areas of the lava lakes were relatively cool. Generally, these areas were the north-eastern region of Main lava lake and the eastern region of Werner's lava lake. The highest temperatures were consistently observed in a southern area of the Main lava lake and near the western and south-western margins of Werner's lava lake.

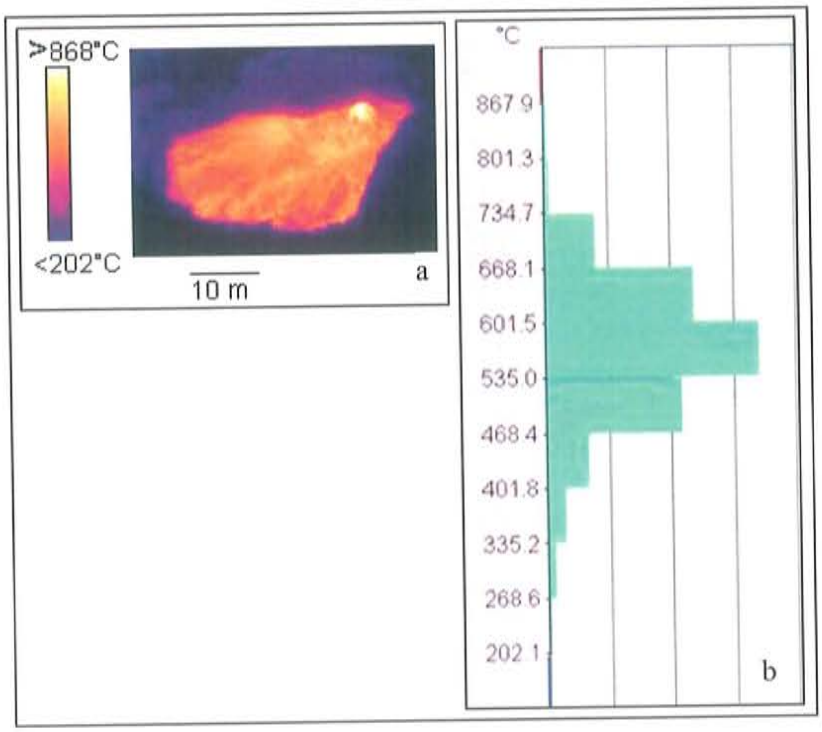

Figure 4. a) FLIR image of Main lava lake with a gas bubble. b) Histogram of pixel temperature distribution from FLIR image. Temperatures are uncorrected and gridlines are increments of 10% of the total number of lava lake pixels.

Surface temperatures of Main lava lake were steady throughout the observation period with averaged daily mean and maximum temperatures remaining within one standard deviation of the mean for the whole dataset. However, surface mean and maximum daily temperatures on Werner's lava lake were observed to increase by more than two standard deviations on 21 Dec, the final day of thermal observations of Werner's Lake. On this day, the maximum temperature observed, on either lake was 923°C for the surface of Werner's Lake. Werner's lava lake formed on 12 Dec 2004 and reached an area of ~1200 m^2 with a daily mean surface temperature of 500°C. Over the next nine days, the lake's northern margin cooled and the actively convecting area of the lake shrunk by 17% to ~1000 m^2. Meanwhile, the daily average maximum temperature of the lake surface rose by 16% from 800 to 930°C and the daily average temperature also rose by 8% from 500 to 540°C.

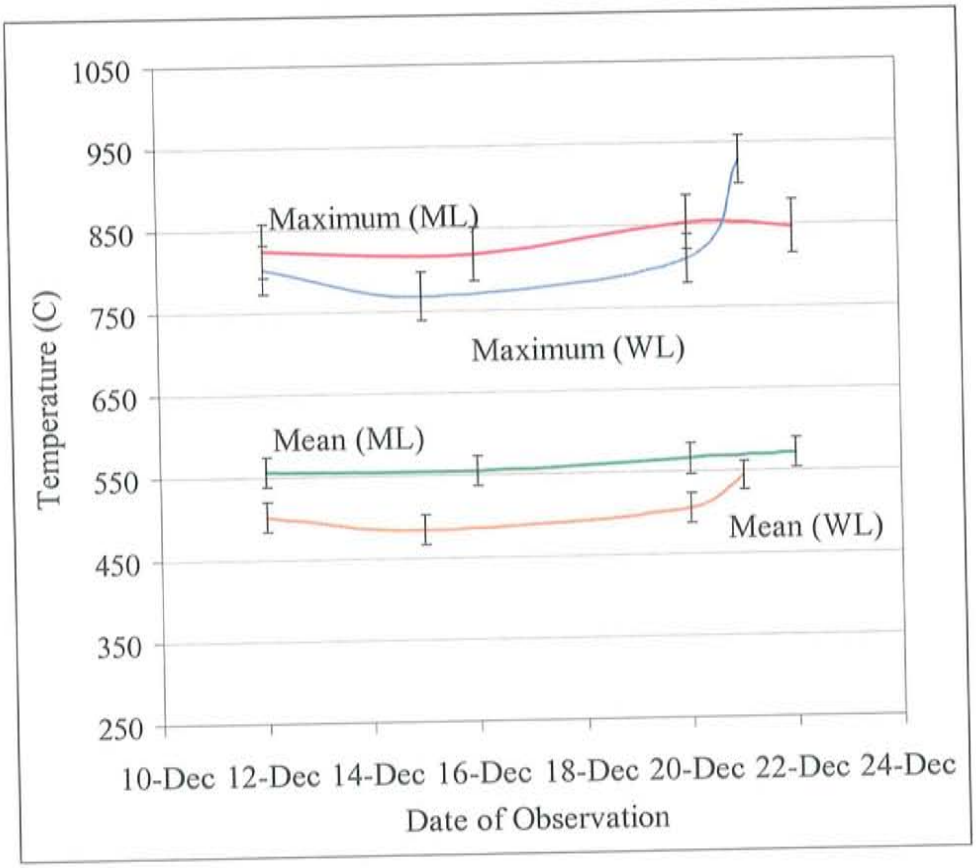

Figure 5. Graph portraying the average daily maximum and daily mean lava lake surface temperatures for the Main Lake (ML) and Werner's Lake (WL). Error bars are ± one standard deviation.

Gas bubbles surfacing and rupturing on the surface of the lake, exposing red, glowing lava, instantly increased mean and maximum lake surface temperatures by up to 40°C and 120°C, respectively. Gases and aerosol emissions from the lava lakes served to lower measured temperatures by intercepting and absorbing lava lake radiation between the lava lake surface and the sensor and significantly lowering transmissivity of the atmospheric path (see Appendix F).

4.1.1 Errors and Corrections to Surface Temperatures

The apparent temperatures recorded by the instrument can be corrected to temperatures of the lake surface taking account of solar radiation reflected from the surface of the lava lakes, the lava surface emissivity, and the absorption of lava lake radiation by gases. Additionally, geometric effects (the oblique viewing angle and variable distance to different parts of the lake) result in range distortions of the imagery. Solar reflectance from the surface of the lakes was not accounted for because the Antarctic summer Sun is only ~15-25° degrees above the horizon at all times and most of the crater floor was in shadow during the times of the thermal observations. In the absence of specific information on the spectral emissivity of active lava at Erebus, surface temperatures reported here were all calculated for an emissivity of 1.0, i.e., they are black body temperatures. The effect of an oblique viewing angle has been neglected because the total effect on heat flux determinations is slight, and is minimized by long occupations of changing areas of incandescence (Oppenheimer and Yirgu, 2002).

More important is the attenuation of radiation (mainly by absorption) along the atmospheric path between lake surface and camera, and a correction is made for this effect. Path amounts of volcanic and atmospheric gases based on simultaneous measurements obtained, from the same observation location, with an open path Fourier transform infrared spectrometer (FTIR) have been used to correct lake surface temperatures. Figure 6 shows the corrected versus uncorrected temperature; note that the correction factor increases with increasing temperature (Sawyer and Burton, 2006) personal communication). Similar results were determined for both lava lakes; details can be found in Appendix F. Correction results show a ~30-70°C (2-8%) underestimate in observed surface temperatures due to volcanic gas attenuation. Because the gas correction cannot be widely applied to the entire dataset, it is used only to approximate the expected offset of temperature and corresponding power output. All other reported temperatures are uncorrected.

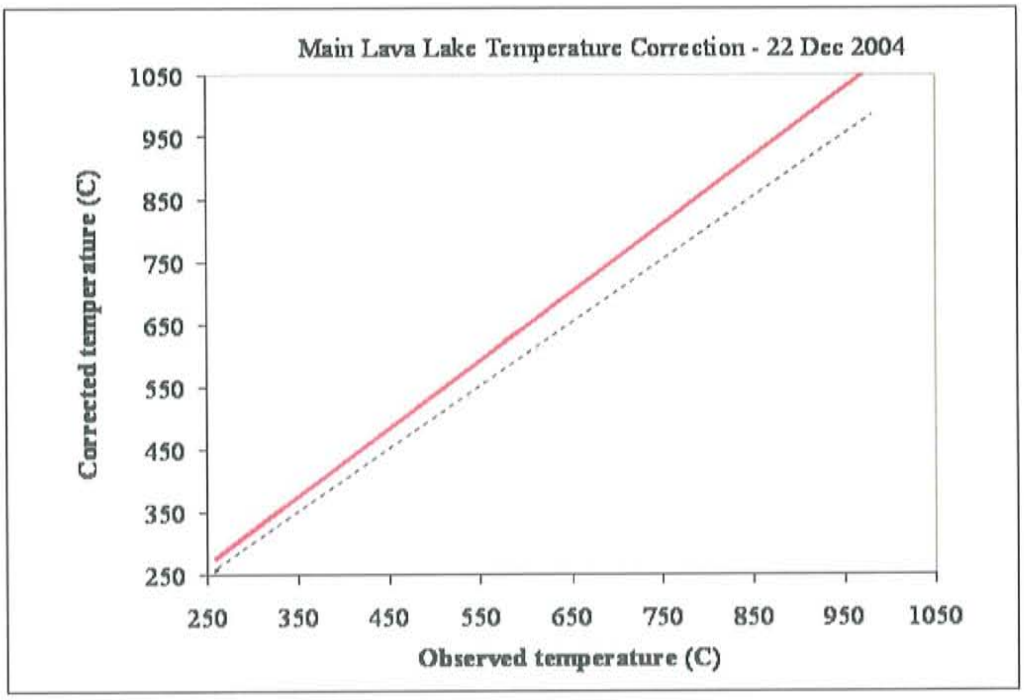

Figure 6. Graph shows corrected surface temperatures. The dashed line corresponds to a 1:1 relationship between observed and corrected temperatures. Gas absorption corrections show a 30-70°C underestimate in observed temperatures.

4.2 Radiative Power Flux

Using the thermal imagery-determined lava lake surface temperatures, the radiative power flux (Q_{rad}) is calculated according to the Stefan-Boltzmann equation:

$$Q_{rad}(\text{Watts}) = \epsilon\ \sigma\ \Sigma\ a_i\ T_i^4 \text{ (evaluated from } i^{th} \text{ to } n^{th})$$

where i equals the first lava lake pixel, and n is the number of lava lake pixels, a_i is the area of the i^{th} pixel in meters square, T is the temperature of the i^{th} pixel in Kelvins, ϵ is the emissivity (here assumed to be 1.0), and σ is the Stefan-Boltzmann constant (5.67×10^{-8} W/m^2K^4). By assuming all pixels have equal area, the area of the lake, A, is defined as: $A = n\ a_i$, reducing the above equation to:

$$Q_{rad}(\text{Watts}) = A\ \epsilon\ \sigma\ \Sigma\ T_i^4 \text{ (evaluated from } i^{th} \text{ to } n^{th}).$$

Many thermal images also contained saturated pixels (>800°C) that were manually added to the image radiative heat flux (Q_{rad}), by assuming a pixel temperature of 923°C (the best estimate of magmatic temperature) resulting in increases of up to 2% to the daily average radiative heat flux (see appendix D for details).

4.2.1 Main Lava Lake

Radiative power output from Main lava lake is ~32 MW ± 3 MW (equivalent to a mean of ~23 kW/m^2 on the lava lake surface). Figure 7 demonstrates the variable

nature of the radiative power output from raw data recorded every 10 seconds. The radiative power averages 30-35 MW, but instantaneous output ranges from 20 to 40 MW or ± 33% around the average. For reference, the average household in the U.S. uses 8900 kW-h annually (Anonymous, 2000). Main Lava Lake, at 32 MW, emits as much radiative power as is consumed by 30,000 homes per year.

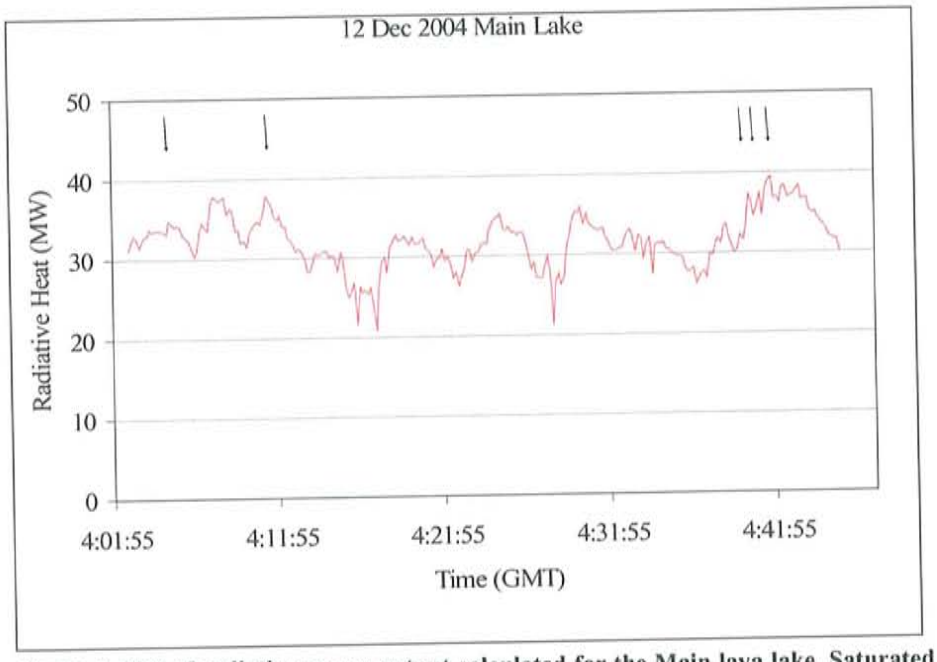

Figure 7. Plot of radiative power output calculated for the Main lava lake. Saturated pixels have been added to values indicated by black arrows (as explained above). Measurements every 10 seconds.

Sudden changes in radiative thermal output were correlated to simultaneous thermal and standard video footage to determine a possible cause. Radiative power output, derived from the thermal camera measurements, is susceptible to changes in atmospheric transmission caused by gases and aerosols absorbing and reflecting emitted radiation between the lava surface and the sensor, as well as to variations in the rate of influx of lava to the lake, the vigour of convection, and the size and frequency of Strombolian bubbles (Fig. 8). A puff of gas drifting across the surface of the lake instantly lowers the perceived lava lake surface temperatures, and

consequently, the calculated radiative power output. This circumstantial effect on transmission and apparent drop in temperatures is not due to any change in lava lake activity. Conversely, a bubble bursting on the lava lake surface significantly increases surface temperatures and the thermal output for up to a minute.

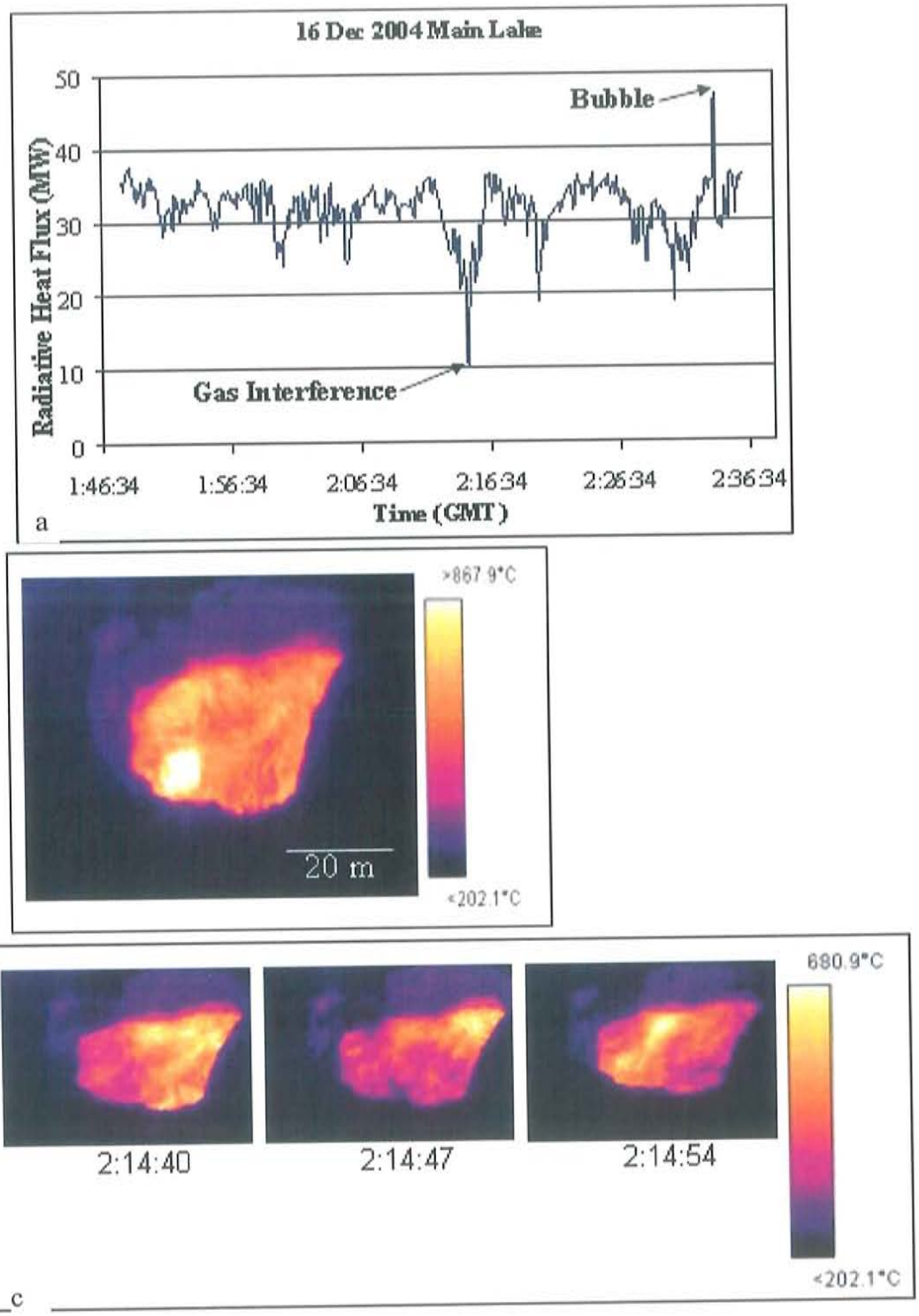

Figure 8. a) Sudden changes in the radiative heat flux due to gas interference and the bursting of a Strombolian bubble on the surface of the lava lake. b) Thermal image of bubble bursting on the surface of the Main lava lake. c) Sequence of images showing a puff of gas affectively cooling the measured lava lake surface temperature as it moves from the left of the image across to exit the frame on the right.

4.2.2 Werner's Lava Lake

Werner's lava lake radiates ~20 MW ± 2 MW consistently, though with the same sudden spikes as observed on the Main lava lake, caused by bubbles and gas and particle absorption (Fig. 9). Werner's Lake is located in the south-western part of the Inner Crater floor and the viewing path was often besieged and blanketed by puffs of gas from the Main lava lake, which pass across the thermal image from left to right, effectively intercepting much of the radiation emitted by the lake. Similarly, the front (northern) edge of Werner's lava lake produced steam clouds on 12 December probably by ingesting snow and/or flowing over cold ground, consequently, a significant amount of gas flowed across the thermal camera field of view.

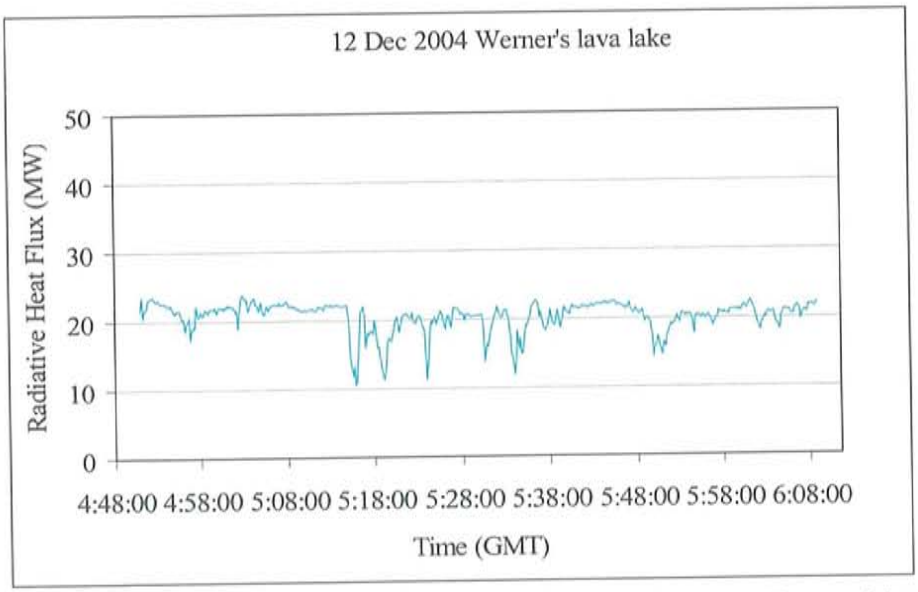

Figure 9. Radiative output of Werner's lava lake calculated from 10 second images. Sudden drops in Q_{rad} are attributed to gas absorption.

Werner's lava lake expanded in surface area on 12 Dec to ~1200 m^2 and gradually shrank to 1000 m^2 over the following 9 days. It is interesting to note that this decrease in area does not correlate to an obvious change in radiative power output (Figs. 9 and 10).

Temporal variations in radiative output are also a qualitative analogy to the energy and dynamism of convection. For example, Werner's lava lake has three sites of upwelling which add material with increasing (or decreasing) vigour over time, inducing more (or less) vigorous convection, exposing the hottest core temperatures of the lava lake, and thereby affecting the radiative output.

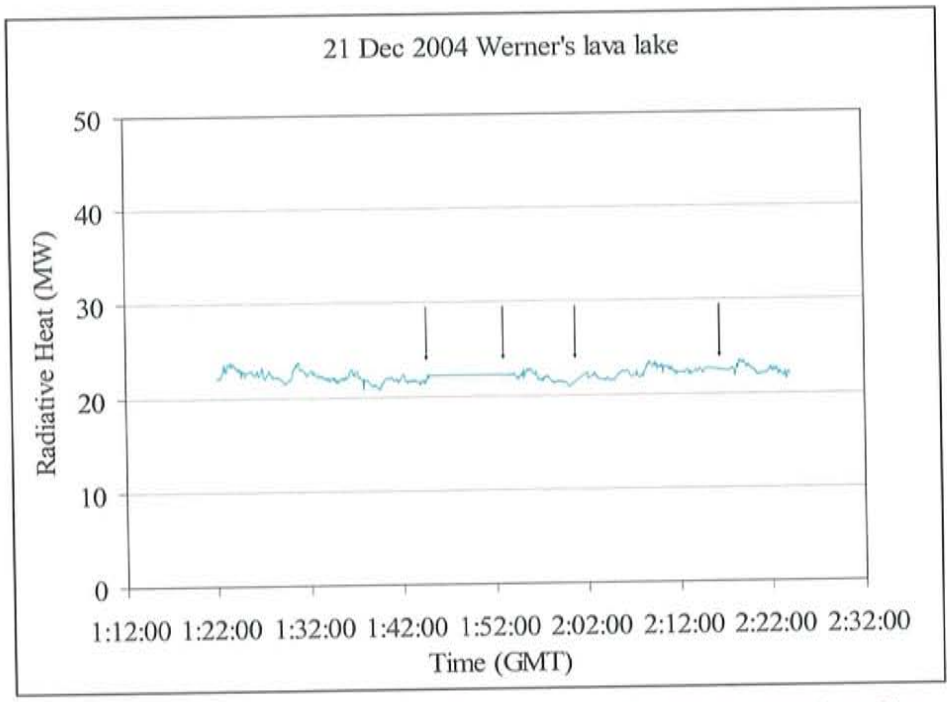

Figure 10. Radiative heat variations of Werner's lava lake due to dynamism of lava convection and influx, not to gas absorption or bubbles. Arrows indicate gaps in record from instrument shutting itself off.

5. Discussion

5.1 Total Lava Lake Heat and Mass Flux

5.1.1 Lava Lake Heat Flux

Total thermal output from Main Lava Lake is defined after Harris et al. [1999] as the sum of radiative heat flux, convective heat flux, and heat carried by the gas phase:

$$Q_{tot} = Q_{rad} + Q_{conv} + Q_{gas}$$

Using the determined lava lake surface temperatures, the convective heat flux (Q_{conv}) is estimated from the formula for free convection from an infinite plate in a half-space as:

$$Q_{conv} = k\,(0.14)\,[(g\,\beta\,Pr)/\nu^2]^{1/3}\,(1.8\,r)^2\,(T_s - T_\infty)^{4/3}$$

Where T_s and T_∞ are the average corrected surface temperature and the ambient (air) temperature, k, Pr, and ν are the thermal conductivity, Prandtl number, and velocity of air, respectively evaluated at the film temperature (T_f), defined as:

$$T_f = (T_s + T_\infty)/2$$

β is the temperature coefficient of thermal conductivity of air, evaluated as:

$$\beta = 1/T_\infty$$

and r is a length scale taken as the radius of the lava lake (see Appendix E for explanation).

Following Harris et al [1999], Q_{gas} is calculated, as:

$$Q_{gas} = F_{gas} c_{gas} (T_m - T_\infty) + F_{H20} L_v$$

where, F_{gas} and F_{H20} are the total gas (exc. water) and total water flux, respectively, c_{gas} is the specific heat capacity (1600 J/kg*K), L_v is the latent heat of condensation (2.26×10^6 J/kg), T_m and T_∞ are the temperature of the magma and the ambient temperature. Using available FTIR gas measurements from the 2004/2005 season, F_{gas}

and F_{H20} are 0.86 kg/s and 9.4 kg/s, respectively (Oppenheimer *et al.*, 2005). Assuming that magmatic temperature is most closely approximated by the maximum temperature recorded during the course of observation, T_m is 990°C, and T_∞ is as defined before, -20°C. The result, Q_{gas} = 22.5 MW, is used as a total for both lakes, and divided between the lakes to report total thermal outputs. Thus, the total thermal output is 47.4 MW from Main Lava Lake and 39.3 MW from Werner's Lava Lake (Table 2).

Table 2. Summary of Lava Lake thermal outputs determined in this study.

	Area (m^2)	*radius* (*m*)	T_s (°C)	Q_{rad} (*MW*)	Q_{conv} (*MW*)	Q_{gas} (*MW*)	Q (*MW*)	Q/m^2 ($x10^{-3}$ *MW/m²*)
Main	1400	20	570	32	4.1	22.5	47.4	33.9
Werner's	1200	19.5	500	20	8		39.3	32.8
Werner's	1000	18	600	20	8		39.3	39.3

Conduction to country rock, for Main Lake is likely to be insignificant: the lake is well-established and insulated. However a newly-formed lake such as Werner's Lava Lake, may have significant conductive heat loss through the conduit and the crater floor to the country rock which cannot be quantified. Nor can fumarolic heat be quantified at this time. Therefore the heat flux values presented here are minimums.

5.1.2 Mass Flux

For a long-lived active lava lake, thermal energy (heat) radiated and convected from the surface of the lava lake must be balanced by heat supplied from the cooling and/or crystallization of buoyant, volatile-rich magma ascending from a reservoir into

the lava lake. Furthermore the steady lava lake level implies that a corresponding flux of degassed, denser magma must be lost from the lava lake. Following Francis *et al.* (1993), the magma flux needed to maintain the total thermal output calculated above is:

$$M = (Q_{rad} + Q_{conv}) / (C_L \Delta f + c_p \Delta T)$$

where C_L is the latent heat of crystallization of the lava (3×10^5 J kg^{-1}), Δf is the crystallized mass fraction (0.3), c_p is the heat capacity of the magma (1150 J $kg^{-1}K^{-1}$), and ΔT is the temperature difference between magmatic and degassed lava exiting the lake (150-200K, as in Harris et al. 1999). Crystallized mass fraction was reported by Kyle (1977) and Dunbar et al (1994) as ~0.3, however it's likely, based on the anorthoclase crystal size (commonly 7-9cm long) and the partially degassed nature of crystal melt inclusions, that circulation within the magmatic system allows for long growth time occurring within the lava lake and within the conduit. Further supporting evidence is suggested by the U-series dating technique which show crystal ages of >100 years according to Sims (*pers. comm. to Kyle*) and 2,380 years as reported in (Reagan et al., 1992). Therefore a Δf of 0.3 is a maximum; assuming that less crystallization is responsible for the lava lake heat flux, possible values are evaluated in Table 4 showing the effect on the calculated mass flux. Mass flux is then calculated as 113-199 kg/s in Main Lava Lake and 88-154 kg/s in Werner's Lava Lake, or a total of 201-353 kg/s for the volcanic system. These values are the minimum magma flux needed to support the thermal output, however they represent minimum values for the system because they take into account only the heat emitted from the surface of the lava lake. Obviously there is material within the lava lake that does not have aerial exposure, does not radiate energy, and therefore is not accounted for in the mass flux as determined.

Table 3. Lava lake mass flux as affected by varying Δf and ΔT. Main Lava Lake (above) and Werner's Lava Lake (below).

Crystallized mass fraction Δf	*Temperature difference* ΔT in K	*Mass flux* M in kg/s
0.3	150	138
0.3	200	113
0.1	150	178
0.1	200	139
0.03	150	199
0.03	200	151

Crystallized mass fraction Δf	*Temperature difference* ΔT in K	*Mass flux* M in kg/s
0.3	150	107
0.3	200	88
0.1	150	138
0.1	200	108
0.03	150	154
0.03	200	117

5.1.3 Previous thermal output determinations

Previous efforts to determine Main Lava Lake's surface temperature and radiative heat flux have been accomplished using geochemical and satellite remote sensing techniques. The first measurements of the lava lake temperature were performed by optical pyrometer and mineral geothermometry (Kyle, 1977; Kyle et al., 1982). Two later estimates were derived from melt inclusion data in anorthoclase crystals, arriving at homogenization temperatures of ~1000°C (Clocchiatti, 1976; Dunbar et al., 1994). Several estimates of lava lake surface temperature and radiative power have emerged from analysis of satellite IR data with results of 900-1130°C and 11-70MW (Table 4)(Glaze et al., 1989; Rothery and Francis, 1990; Harris et al., 1997; Harris et al., 1999a; Wright and Flynn, 2004; Davies et al., 2005, submitted).

Table 4. Summary of results of previous thermal studies on Erebus volcanic activity.

Date[a]	Technique	Lake size ($m^{2)}$	T_L (°C)	Q_{rad} (MW)	Q_{tot} (MW)	Reference
1976	Optical pyrometer	~2800 (30 m radius)	980±20	---	---	(Kyle et al., 1982)
1977	Geothermometry	~2800 (30 m radius)	1000	---	---	(Kyle, 1977)
1976	Melt inclusions	---	980-1030	---	---	(Clocchiatti, 1976)
1985	Landsat TM	~180	900-1130	---	---	(Rothery and Francis, 1990)
1994	Melt inclusions	---	975-1000	---	---	(Dunbar et al., 1994)
1985	Landsat TM	180	1000*	12-18	16-103	(Harris et al., 1999a)
1989	Landsat TM	300	1000*	8-15	13-108	
1980	AVHRR	~4500	1000*	60-70	80-110	(Harris et al., 1997)
1980	Landsat TM	~4500	---	58	---	(Glaze et al., 1989)
2002	MODIS	(5-15 m diam.)	1000*	22**	---	(Wright and Flynn, 2004)
2003	HYPERION	2125	---	18.1	---	(Davies et al., 2005, submitted)
2004	Ground-based IR	1400/1000	990	52#	87#	This study

*Lava lake temperature assumed from Kyle, 1977.

**Annual average, with monthly estimates from 10-80MW.

#Sum of values for both lava lakes present in 2004.

In comparison, the values determined from this study (of maximum lava lake surface temperature of 990°C, Q_{rad} of 32 and 20 MW, and Q_{tot} of 47 to 39 MW for Main and Werner's Lava Lakes, respectively) are well within range of previous estimates, though considered to be far more accurate. Contraction and growth of the lava lake affects the radiative and total thermal output, whereas lake surface temperatures are relatively constant in all reports. Furthermore, thermal flux determined here are 0.02 MW/m^2 radiative heat and 0.03-0.04 MW/m^2 total heat, which is also comparable to previous thermal studies, taking into consideration changes in surface area of Main Lava Lake over time. Werner's Lava Lake being

newly formed and ephemeral, no previous studies exist for comparison. Effects of changes in the magma supply rate, and therefore heat, can be dampened due to the geometry of the Main Lake's pit crater. However, for Werner's Lake, changes in magma supply and heat have been observed or can be assumed to occur as this lava lake flowed out and dammed itself.

5.1.4 Previous mass flux determinations

Harris et al (1999), using Landsat TM data, determined a mass flux for Erebus lava lake as 38-76 kg/s and 30-69 kg/s, for 1985 and 1989 respectively. The lava lake, at the time of the Landsat TM image retrievals, was of considerably less area than either of the lakes present in 2004. Though the power outputs determined in this study are greater, the mass flux per unit area is comparable at 0.1-0.2 kg/s-m^2.

5.1.5 Comparison to Erta Ale lava lake

Sustained lava lake activity also occurs at Erta 'Ale Volcano, Ethiopia, and Nyiragongo Volcano, Democratic Republic of Congo. However, Nyiragongo Lava Lake, located in a politically unstable country, has not been the subject of published ground-based thermal observations. Erta Ale Lava Lake has been thermally investigated in recent years using ground-based infrared imaging instruments and an optical pyrometer (Burgi et al., 2002; Oppenheimer and Yirgu, 2000; Oppenheimer et al., 2004). The quantitative results are summarized in Table 5.

Table 5. Summary and comparison of ground-based thermal results on Erta 'Ale lava lake.

	T_{max} (°C)	Q_{rad} (MW)	M (kg/s)	A (m^2)	$Q_{rad}/Area$ (MW/m^2)
Erta 'Ale[a]	1100-1200	70-150		6200	0.011-0.024
Erta 'Ale[b]	1187	110	510-580	6200	0.018
Erta 'Ale[c]	>1000	5-30	350-650	910	0.005-0.033
Erebus[d]	990	20-32	88-199	1000-1400	0.020-0.023

[a]Oppenheimer and Yirgu, 2002

[b]Burgi et al, 2002 (non-imaging technique)

[c]Oppenheimer et al, 2004

[d]This study

The surface of Erta Ale lava lake appears smooth, with plates of cooler lava (~480-500°C) separated by incandescent ridges of 1100°C. The smooth surface is interrupted sporadically by vigorous overturning. This is in contrast to the surface observations of Mount Erebus lava lake, where vigour remains relatively high near the sites of upwelling.

5.2 Visual Observations and Interpretation

5.2.1 Main Lava Lake

The convection pattern in Main Lava Lake is controlled by an upwelling source in the southern-central area of the lake (Fig. 11). Upwelling material then appears to flow radially outward from the source. A second flow direction is sometimes seen which is characterized by lava from the left side of the source area, flowing over and against the right side, sometimes creating a seam, bisecting the source area, of lava flowing in both directions. A 500°C platy crust frequently builds up along the north-eastern shore when movement on the lake appears to slow, and flowing material disappears beneath

the edge of the plates. When flow picks up speed again, the plates either get swamped, founder, and disappear or are knocked loose in pieces and drift away from the margin, staying intact for a few more minutes, before being reassimilated into the molten lake.

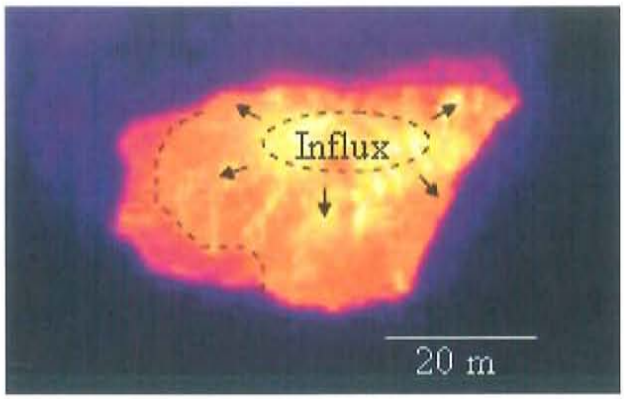

Figure 11. The upwelling source of Main Lava Lake (dashed oval) is the site of the highest surface temperatures. Arrows show general flow pattern and dashed line indicates area of plate build-up.

Bubbles generally appear near the margin of the lava lake in the northern area of the lake (lower left of Fig. 11) and in the area south of the influx (upper right). They burst on the surface about every 5 minutes and can appear in thermal images for up to 30 seconds though the increase in temperature (and radiation) can last for 1-2 minutes. Bubbles range in area from less than 1 m^2 to 60 m^2 (shown in Fig. 8b). Velocity of the lake surface, determined by tracking surface material in The Environment for Visualizing Images Software (ENVI) using the measurement tool and the known time between image acquisitions, ranges from ~0.8 m/s near the source area to $\leq$ 0.1 m/s near the lake margin.

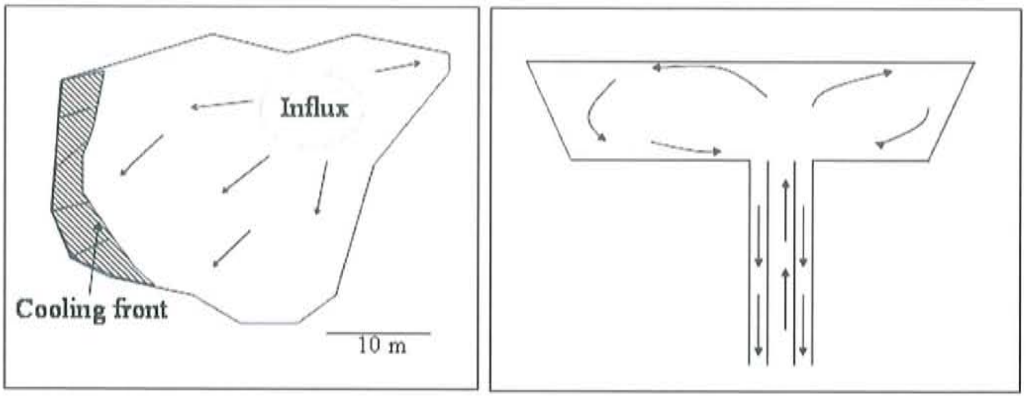

Figure 12. Schematic diagram of Main Lava Lake system in a) plan view showing vectors of surface motion and b) cross-sectional view showing inferred convection cycle.

5.2.2 Werner's Lava Lake

There are three areas of upwelling feeding Werner's Lava Lake identifiable on the thermal images: the flow of lava joining the lake at the south-western margin (upper right), a lake source in the southern area, and a lake source in the north-western quadrant of the lake (Figs. 13 and 14). Convection is characterised by upwelled material moving out from the sources into the main body of the lake and then pushing to the eastern margin and disappearing (downwelling?). Frequently, lava also appears to be flowing out of the lava lake at the southern sub-lake source. Plates of cooler material often formed at the site that later became completely solidified. These slabs cool to ~ 450°C, and eventually founder and sink into the lake after as much as 10-12 min.

Bubbles burst at the surface of Werner's Lava Lake every ~3 min., more often than on Main Lava Lake, and are concentrated near the eastern lake edge and the upwelling sites. Rates of movement on the lake surface are somewhat higher than that of Main Lava Lake: >1 m/s near the southern inflow and <0.3 m/s near the margins.

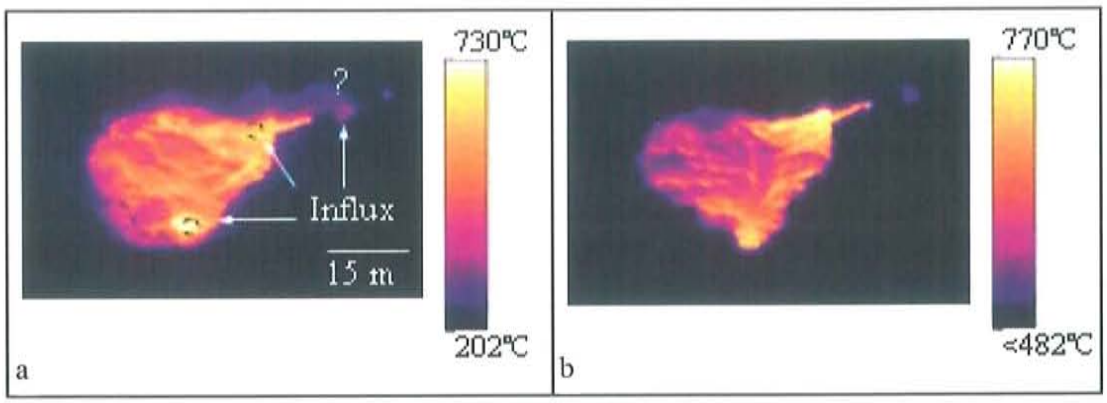

Figure 13. Three locations of upwelling are shown as dashed circles for the two that are visible and a question mark for the flow of lava that is assumed to be hidden by a rock outcrop. a) 12 Dec 2004, cooled area is indicated by a dashed line near the northern source. b) 21 Dec 2004

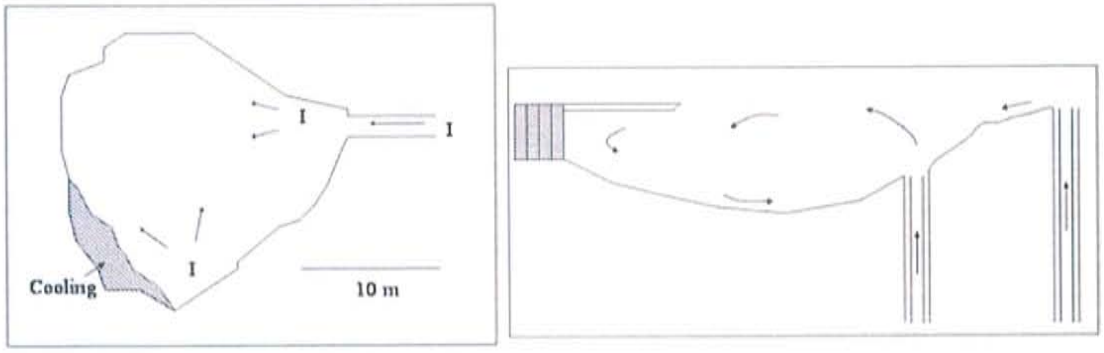

Figure 14. Schematic diagram of Werner's Lava Lake in a) plan view showing vectors of surface motion and sites of upwelling and b) cross-sectional view showing inferred convection cycle.

Werner's lake was observed to shrink in area over a 9 day period, resulting in a 200 m^2 decrease in surface area (Figs. 13 and 15). As can be observed in fig 13a-b., a lower left portion of the lake cools to the point of being indistinguishable from background temperatures between Dec 12 and Dec 21. Furthermore, the radiative thermal output remained steady despite the decrease in surface area and the lava lake surface temperatures were observed to increase by an average of ~50°C. Possible explanations for this include increased transmission (crater clarity), increased vigour

of circulation and exposure of fresh magma at the surface, or the effect of the lava lake system becoming thermally insulated, thereby decreasing conductive losses.

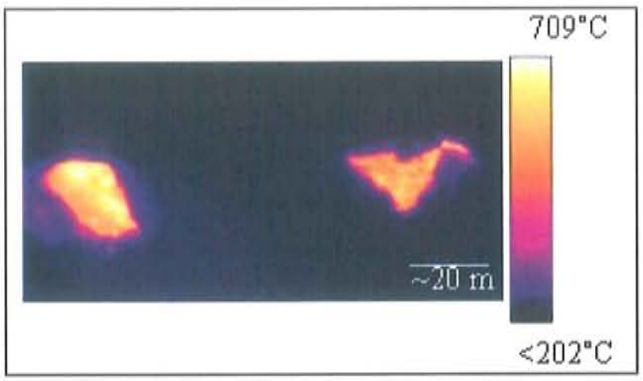

Figure 15. 21 Dec 2004 Thermal image of both lava lakes, taken from helicopter: Main Lake on the left and Werner's Lake on the right.

5.3 Volcanological Implications

5.3.1 Magma and lava lake system

Between eruptive cycles, volcanoes can exhibit persistent steady-state open vent activity (Harris and Stevenson, 1997; Stevenson and Blake, 1998; Slezin, 2003). Lava lakes are the surface expression of an apparently steady-state volcanic system. With little or no eruptive material, long-lived lava lake systems are indicative of efficient convective circulation linking surface activity to a deep reservoir of magma. Because there is a constant heat flux with no substantial net change in the level of the lava lake, material must be drained out of the lake as steadily as it is injected.

Magma ascending to the lake is volatile-rich and near magmatic reservoir temperatures, assuming some slight (tens of degrees) cooling during the ascent (Stevenson and Blake, 1998; Slezin, 2003). Magma depressurizes and degasses at shallow depths, with gas exsolving and either, separating from the liquid phase with a greater ascent velocity, or by in-situ bubble growth, forming closely-packed bubbly layers (foam). These two scenarios are modelled, respectively, as the discrete gas

separation regime and the dispersion regime of Slezin (2003). Erebus activity is typified by large gas bubbles separate from liquid flow, promoting the discrete gas separation regime as the better fit. Rising magma continues to degas and cool within the lava lake, becoming denser, more viscous, and eventually sinking, thereby driving convective overturn. This system of convection, driven by degassing, has been modelled as a bi-flow conduit (Fig. 16) by Kazahaya *et al.* (1994), Stevenson and Blake (1998) and Huppert and Hallworth (2006).

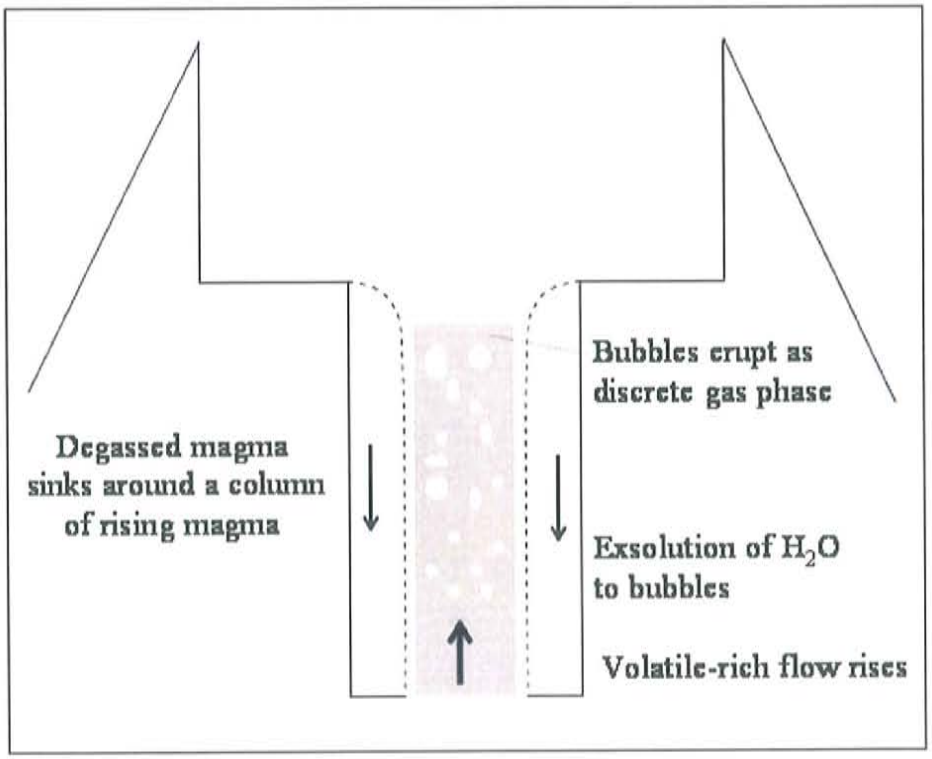

Figure 16. Cartoon of convection driven by degassing in a bi-flow conduit with discrete gas bubbles (after Stevenson and Blake, 1998; Slezin, 2003)

Is a conduit necessary to explain the activity of a long-lived lava lake like exists at Erebus? The Erebus lava lake system can be modelled either as the surface feature of a bi-flow conduit containing magma ascending and descending from a magma reservoir (Fig. 17a), or as the exposed top of a circulating magma reservoir (Fig. 17b).

In the former model, the conduit provides hot, gassy, buoyant material and disposes of cooled, dense, degassed material. By following Kazahaya et al (1994), the minimum radius of the conduit needed to supply 150 kg/s to the Main Lake can be found by:

$$Q = (\pi \Delta\rho \, g \, r_a^4) / 8\mu_a$$

where Q is the ascending magma flux (150 kg/s), $\Delta\rho$ is the difference in density between ascending and descending magma (70 kg/m^3), g is gravitational acceleration (9.8 m/s^2), r_a is the radius of the ascending (inner) conduit, and μ_a is the viscosity of the ascending magma ($10^{3.2}$ Pa-s). Assuming that the minimum amount of material in the lava lake system must be 150 kg/s ascending and descending, this bi-flow can be supported by a conduit ~2 m in radius.

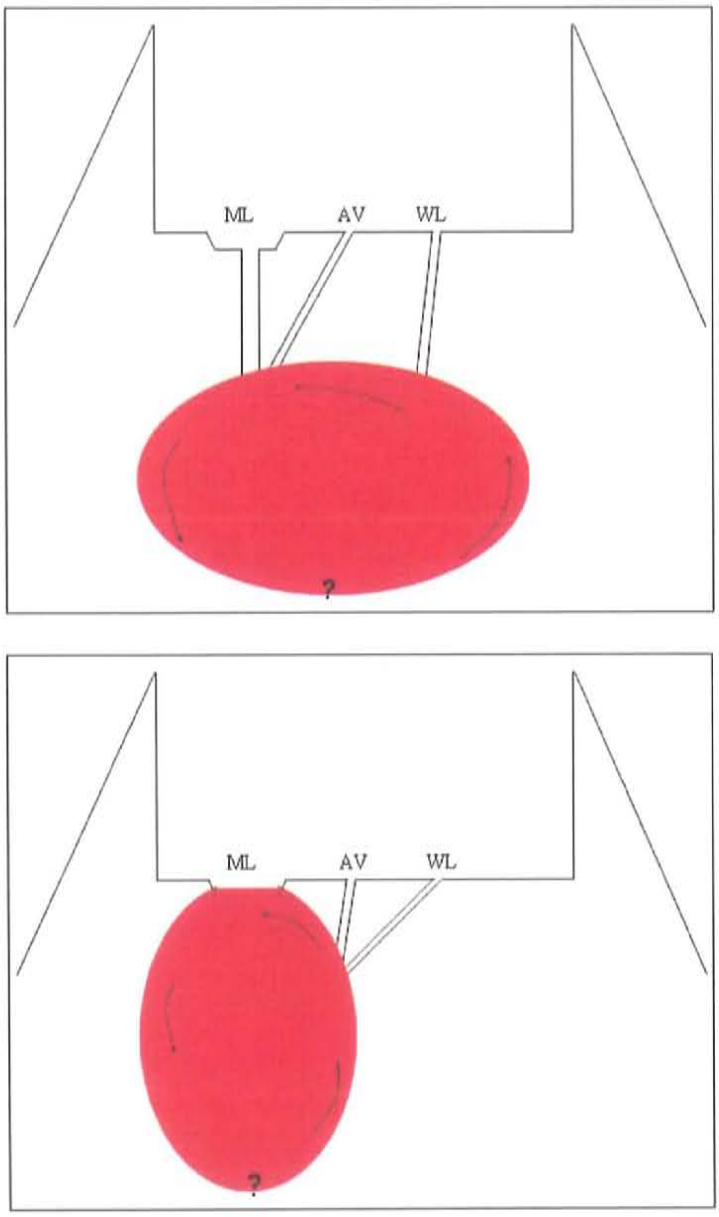

Figure 17. a) Lava lake model with bi-flow conduits connecting magma reservoir to Main Lake (ML), Active Vent (AV), and Werner's Lake (WL). b) Lava lake model with Main Lake as the exposed top of the magma reservoir, and conduits linking Active Vent and Werner's Lake to the magmatic system.

However, as previously stated this accounts only for the magmatic material that is exposed on the surface. If, as in the second scenario (fig. 17b), the lava lake is the exposed top of a magma reservoir than the 'conduit' radius could be considered the

radius of the lava lake (21 m). The inner conduit could supply a maximum of 3.45 x 10^6 kg/s (1330 m^3/s) of ascending magma to the lava lake. I suspect that the true magma flux is closer to the maximum, because as eruptions occur displacing material in the lava lake, the level of the lake does not appear to change. An explosion that lowered the level of the lava lake by 1 cm (displaced 14m^3 of material), if instantly recovered, would be accounted for by a magma flux rate of 36,000 kg/s. If the magma flux rate were 150 kg/s, this 1 cm rebound would take 4 minutes. Another way of parameterizing is to assume that the lava lake is at least 1 m deep, therefore the minimum volume of the lava lake is 1400 m^3 (3.6M kg). If we also assume that the surface of the lava lake responsible for the heat output is 1 cm thick or represents 3.6 x 10^4 kg of material, then the thermal output is derived from 1% of the lava lake volume.

5.3.2 Mass Balance Models

To maintain steady-state lava lake activity a constant supply of magma is necessary to thwart cooling and solidification, and a constant drain of magma is necessary for mass balance. The fate of the descending cooled material is conventionally believed to either be recycled to the magma reservoir, where it incrementally induces cooling, or removed from circulation by intrusion. If reservoir cooling is used to balance heat and mass supplied to the lava lake, then after Harris et al (1999),

$$Q_{rad} + Q_{conv} = M_{res}\, \Delta T_{res}\, c_p$$

Where M_{res} is the volume of the reservoir and ΔT_{res} is the change in temperature of the reservoir induced by heat loss. Using just the heat lost from Main Lake, a 0.4°C of cooling would be induced annually in a 1 km^3 reservoir or ~12°C in 32 years of

persistent lava lake activity. Therefore in a 1 km^3 reservoir which is likely no more than 10°C above liquidus temperature, 12°C of cooling would result in the onset of sustained crystallization after only 25 years. Add to that the heat loss from Werner's Lava Lake and Active Vent, and significant changes to the reservoir and thermal output would have been observed. Therefore it is unlikely that the reservoir could be that small. However a 2 km^3 or larger magma reservoir could sustain Main Lake heat flux for at least 210 years, before the onset of sustained crystallization, and without the need for intrusive growth activity.

Intrusive growth as a means of disposing of cooled degassed material can be either cryptic or endogenous (Francis et al., 1993; Allard, 1997; Oppenheimer and Francis, 1998). Endogenous growth of the edifice induced by intrusion is likely to cause uplift and deformation on the surface. As no such deformation has been observed, the possibility of endogenous growth is negated and cryptic growth remains a viable intrusive model. Furthermore, Dunbar et al (1994) propose multi-stage crystal growth process including resorbtion based on anorthoclase crystal chemistry. The recycling of crystals is evidence against magmatic intrusion and removal of material from the system, and rather, supports steady circulation of magma.

6. Conclusions

Herein determined radiative and total heat flux of 47 MW and 39 MW, respectively, for the two Mt. Erebus lava lakes is based on the only current ground-based thermal data and is also, the most accurate estimate of thermal output to date. The convection of Erebus lava lakes is supported by crystallization and heat lost from the lake surface. By calculating the mass flux necessary to sustain this heat loss, the minimum volume of the reservoir and the minimum radius of the conduit are reported as 2 km^3 and ~2 m, respectively. The quantitative conclusions from this study also serve as a basic comparison to and a calibration for heat loss determinations derived from space-based imagery, such as Hyperion, Moderate Resolution Imaging Spectroradiometer (MODIS), and Advanced Space-borne Thermal Emission and Reflection Radiometer (ASTER). Furthermore, qualitative deductions derived from this data have greatly improved knowledge of the locations of upwelling, and bubble bursts, the frequency of events, and the rates of movement across the lake surfaces. This study will be continued by the addition of more recent data which will likely further supplement our understanding of strombolian and lava lake eruption cycles.

Appendix A. Infra-Red Radiometry and Thermography

A.1 Introduction

This appendix is designed to introduce the reader to the basic principles and laws that govern the work described in the main body of the thesis. To understand the significance and merit of this research, it is useful to gain a basic background in radiation theory and infrared radiometry.

A.2 Blackbody Radiation

All matter continuously emits energy in thermal IR wavelengths (3-14um). How much energy an object emits is a function of the object's surface temperature. A blackbody is a theoretical object that:

- absorbs all incident radiation, regardless of wavelength (λ) or incident direction,

-emits more energy for a given λ and temperature than any other surface

-emits radiation irrespective of direction (Lillesand and Kiefer, 2000)

A black body is a perfect absorber and radiator and therefore, is useful as a standard to which real object radiation can be compared. The spectral radiative power of a blackbody at some temperature, T, is given by Planck's distribution equation:

$$E_{\lambda,b} = C_1/[e^{\wedge}(C_2/\lambda T)-1] \quad (1)$$

Where constants $C_1 = 3.742 \times 10^8$ W-$\mu m^4/m^2$ and $C_2 = 1.439 \times 10^4$ μm-K

Planck's distribution is also shown graphically as blackbody radiation curves in Fig. A1.

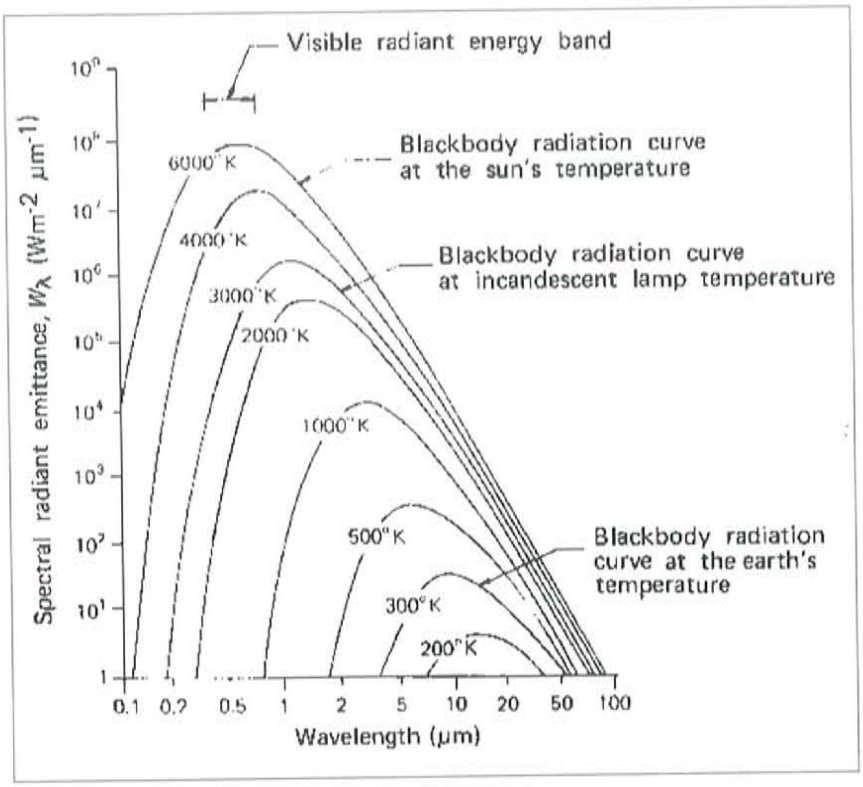

Figure A1. Planck's distribution curves showing blackbody radiance at various temperatures (Lillesand and Kiefer, 2000)

From Planck's distribution curves, it can be observed that objects as temperature increases more energy is radiated at shorter wavelengths. This relationship is also established by Wien's displacement law (equation 2), which states that for a body at temperature, T, the wavelength at which maximum radiation occurs varies inversely with the absolute temperature of the body (Lillesand and Kiefer, 2000).

$$\lambda_{max} = (2.898 \times 10^{-3}\ \text{K-m})/T \qquad (2)$$

The final part of blackbody radiation theory is the Stefan-Boltzmann law, which results from integrating Planck's distribution equation (1) over all wavelengths:

$$E_b = \sigma T^4 \qquad (3)$$

where the Stefan-Boltzmann constant, σ equals 5.67×10^{-8} W/m^{2}K^4. The Stefan-Boltzmann law simply states that total radiation flux from a blackbody (E_b) is directly

related to the fourth power of the absolute temperature (T) of the blackbody (Lillesand and Kiefer, 2000)

A.3 Real Object Radiation

A real object is imperfect and hence, does not act exactly as a blackbody, though for simplicity, a blackbody is often used to approximate a real object. For calculating real object radiation, we adjust the blackbody radiation by a quantity, the emissivity (ϵ), which is a ratio of the total radiative power of the real object of interest (E_r) to the total radiative power of a blackbody (E_b) at the same temperature.

$$\epsilon = E_r / E_b \quad (4)$$

Hence the emissivity of a real object is between 0 and 1, and a real object with near blackbody behavior will have an emissivity approaching unity. Therefore, in terms most relevant to this study, blackbody radiance is related to actual lava lake radiance via the emissivity. The Stefan-Boltzmann equation is then modified to account for emissivity and becomes:

$$E_r = \epsilon \sigma T^4 \quad (5)$$

A.4 Infrared Radiometry

An IR radiometer is a device that measures radiative electromagnetic energy in the infra-red wavelengths (0.75μm -1000μm [1mm]). The Agema Thermovision 550 camera, used in this study, measures and images emitted short-wave infrared radiation of 3.6-5.0μm. Target radiation is received by a sensor within the instrument, which processes the data by applying the Stefan-Boltzmann law and the set emissivity(5). The Stefan-Boltzmann law is used to find the temperature correlating to the amount of radiance received by that sensor. To calculate the total radiative heat flux of the

source, the T^4 of all the lava lake pixels are summed and multiplied by the area of the lava lake,

$$Q_{rad}\ (watts) = A\ \epsilon\ \sigma\ \Sigma T^4 \quad (6)$$

where A is the area of the lava lake in square meters, ϵ is emissivity (= 1 in this case), and σ is the Stefan-Boltzmann constant, $\sigma = 5.67 \times 10^{-8}\ W/m^2K^4$. Table A1 serves to summarize the total radiative heat flux calculation.

Table A. 3 Summary of calculations from radiometer measured radiance to total radiative heat flux.

1. Calculating the radiative heat flux of a pixel	A sensor measures the amount of radiance $(Q_{rad})^*$ received and solves for the temperature (T) of the pixel by using the Stefan-Boltzmann law and the set emissivity: $Q_{rad}\ (watts/m^2) = \epsilon\ \sigma\ T^4$
2. Calculating the radiative heat flux from the lava lake	The pixel temperatures are summed to calculate Q_{rad} for the entire lava lake by using $Q_{rad}\ (watts) = A\ \epsilon\ \sigma\ \Sigma T^4$, where A is the lava lake area in square meters.

* In IR radiometry 'Q_{rad}' is conventionally signifies radiative heat flux, instead of E_r.

Appendix B. Thermal Camera Instrument Specifications

FLIR stands for Forward Looking Infrared Radiometer. Like GPS, radar, and other satellite-based techniques, the FLIR is a target locating device first developed for the military. The technology was declassified in 1968. The development company FLIR Systems quickly seized the market: manufacturing both instrument and software. FLIR is now being incorporated into many scientific disciplines including medicine and animal behavior research.

Thermal observations of the lava lakes were made with a tripod-mounted Agema Thermovision 550 infrared camera. It is a stirling-cycle cooled focal plane array infrared radiometer, with PtSi sensors arranged 320 by 240. The sensors are responsive from 3.6-5.0μm. The camera measures temperatures from 0°C to 1200°C and is calibrated by an internal temperature reference, consisting of three filters: 0-400°C, 250-800°C, and 600-1500°C, also called throughout this study as low-, medium- and high-range filters, respectively. The majority of the thermal observations in this study were acquired with the medium-range filter, though a few sets of images were acquired with the high-range filter. The thermal camera has a 20° x 15° field of view, which corresponds to an instantaneous field-of-view (IFOV) of 1.1mrad, and to 0.42m x 0.42m pixels for the Main Lake and 0.41m x 0.41m pixels for Werner's Lake (see Appendix C for a discussion of the pixel size calibration).

Table B4. Thermal camera instrument specifications

Wavelength range	3.6-5.0μm
Temperature range	0 - 1200°C
Measurement Accuracy	± 2%
Thermal Sensitivity	< 0.1°C
Field of View	20° x 15°
Detector Type:	FPA 320 x 240

FPA = focal plane array

Appendix C: Determination of Lava Lake Areas

C.1 Introduction

Uncertainty in the pixel size of recorded thermal images and the surface areas of the two lava lakes observed in December 2004 are the largest source of error in the radiative heat calculations. This error in turn propagates into calculations of the lava lake heat and mass fluxes. A number of attempts have been made to accurately determine the areas of Main and Werner's lava lakes and these are described below.

C.2 Lava Lake areas calculated using laser range-finding (LRF) binoculars

C.2.1 *2004 measurements*

On 12 December 2004, P. Kelly used laser range finding binoculars (Leica LRF 800) and a clinometer (Suunto PM-5/360) to measure distances and viewing angles to the edge of Main lava lake from the Main Crater rim (Kelly, *pers. comm.*, 2005). These measurements gave a maximum radius of ~21 m for the lake. Assuming Main lava lake was circular it had a surface area of ~1400 m^2 (Table C 1). Werner's lava lake surface area was estimated in a similar manner. On 12 December 2004 it had a radius of ~19.5 m this gives a surface area of ~1200 m^2 for a circular lake. On 21 December 2004 the radius was 18 m and the area ~1000 m^2 (Table C 1).

Table C1. Summary of the methods used to calculate the lava lake areas and the corresponding results from each of the methods. Errors are estimated from instrument and method precision and accuracy. 'Year' column lists the year the data was collected for the area determination.

Year[a]	Method	Calculated Area Main Lake	Calculated Area Werner's Lake[b]	Error[c]
2001	ENVI measuring tool on DEM	1300m^2	N/A	± 1%
2003	LRF measurements	1630m^2	N/A	± 100m^2
2004	LRF measurements	1400m^2	1300-1000m^2	± 100m^2
2004	IFOV of thermal camera	~900m^2	~800m^2	?± 200m^2
2004	Hyperion Thermal Imager	~2100-2200m^2	<825m^2(vent)	unknown

[a] 'Year' column lists the year the data was collected for the area determination.
[b] Werner's Lake is x-x% of the area of Main lava lake.
[c] Errors are estimated from instrument and method precision and accuracy.
ENVI = The Environment for Visualizing Images
DEM= Digital Elevation Model
LRF – Laser-range finder
IFOV = Instantaneous field-of-view

C.2.2 *2003 measurements*

In December 2003, C. Oppenheimer used laser range finding binoculars (Leica Vector) to measure distances to the Main lava lake from the Main Crater rim (Oppenheimer, *pers. comm.*, 2005). From these measurements and the measured viewing angles, the maximum radius of the lake was calculated as ~22.7 m giving a maximum area for Main lava lake of ~1630 m^2. The area of Main lava lake was greater in December 2003 compared to December 2004 as there was an obvious drop in the height of the lake between the 2003/04 and 2004/05 field seasons. The greater surface area in 2003 is therefore consistent with the 2004 area values calculated above.

C.3 Lava lake areas calculated using the IFOV of the thermal camera

The instantaneous field-of-view (IFOV) of the thermal camera instrument is 1.1mrad. The LRF measurements made in 2003 (see C.2 above) gave the path length to the lava lake and the altitude above the lake as ~300m and 200m, respectively. Using the IFOV and the LRF data the footprint on the surface of the lava lake was determined as shown in Figure C 1, with approximate pixel counts for Main and Werner's Lake of 7200 and 6300 pixels, respectively. This gives an area of Main lava lake of ~900m^2 and a maximum area of Werner's lava lake of 800m^2 (Table C 1).

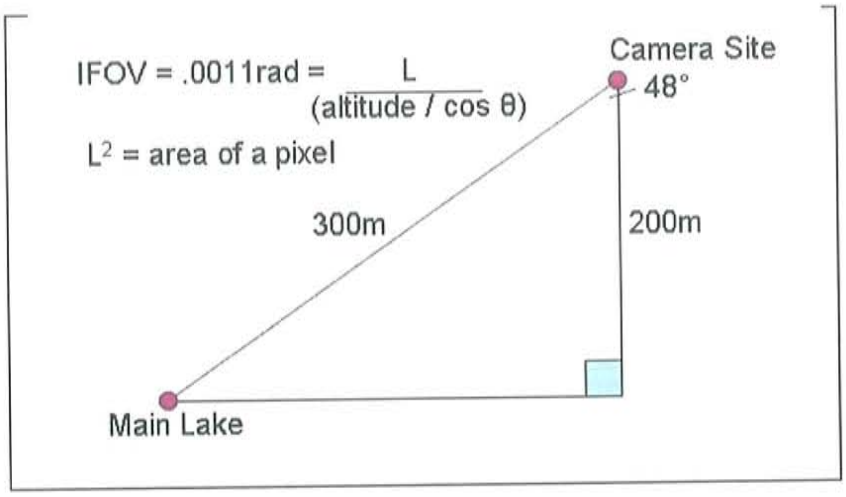

Figure C3. The area is calculated using the IFOV of the thermal camera instrument, the altitude determined by another method, and the viewing angle determined geometrically. (Lillesand and Kiefer, 2000)

C.4 Lava Lake areas calculated from Digital Elevation Model

A digital elevation model (DEM) of Mount Erebus volcano was constructed using data obtained by NASA's Airborne Topographic Mapper (ATM) scanning laser altimeter in 2001 by USGS (http://usarc.usgs.gov/ant-ogc-viewer/lidardownload.htm). The DEM is a single-band very high-resolution image (2m x 2m cell size) of the study area, which is geographically referenced to the earth. Main lava lake was identified in the DEM and the area measured using ENVI's polygon measuring tool; the area measured for the Main Lake was ~1300m^2. Werner's Lake was not yet formed at the time of image acquisition. The DEM is useful as an extremely accurate measurement of distance and elevation with a relative accuracy of $\pm$ 0.1m and absolute accuracy of $\pm$ 2m.

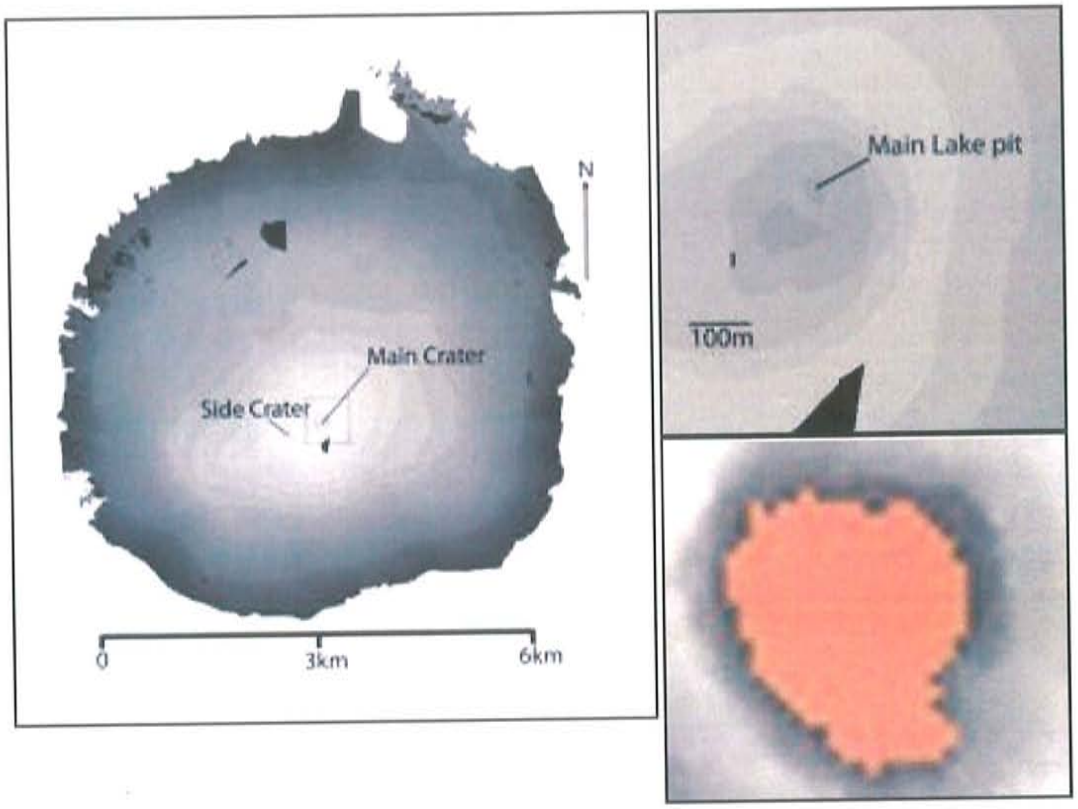

Figure C4.

A)The Digital Elevation Model of Mount Erebus with a 50m contour interval. B) The Inner Crater floor area. C) Pixels within Main lava lake (orange) have been chosen by their elevation and the lava lake area calculated as 1300m^2. In December 2001 Main lava lake was at an elevation of 3515-3519m.

C.5 Lava Lake areas reported in recent literature

In a demonstration of the volcanism detection applications of Hyperion Thermal Imager on board EO-1, Davies et al. (2005) detected two thermally active areas on 7 May 2004 within the Inner Crater of Erebus Volcano. Main lava lake was reported to radiate 18.1MW from a thermal output source of 2185m^2, whereas Werner's lava lake/vent radiated 6.1MW from an area of 825m^2 (Davies et al. 2005,). Data from this study was used to estimate a Main lava lake radius of 26m^2 (Davies, *pers.comm.*, 2005).

C.6 Conclusions

Despite the greater accuracy of lava lake areas calculated from the DEM, I have used the value 1400m^2 for the area of Main lava lake and 1300-1000m^2 for Werner's for all calculations, based on the most recent LRF measurement. As stated in C.2 above, these measurements were simultaneously obtained with thermal observations.

The size of the individual pixels in the thermal images were calculated using the 2004 lava lake surface area measurements as .42m x .42m on Main lava lake and .41m x .41m on Werner's lava lake. These values were used throughout this study because they are the only set of measurements contemporary with the collection of thermal imagery, as well as the only measured values for the newly-formed Werner's lava lake.

Appendix D: Image Recording and Data Processing

D.1 Image Recording

Data were recorded using the standard FLIR software program ThermaCAM Researcher 2002. Images were recorded as time-stamped ThermaCAM Image files, with a 1-10 second frequency using either the mid-range or high-range filter (see Appendix B for instrument specifications). Sustained observations were up to an hour in length, and were unexpectedly terminated when the thermal camera shut itself off periodically. This technical problem may have resulted from operating in the extremely low ambient temperature (<0°C), though the instrument was outfitted with extreme cold-weather protection in the form of duct tape and layers of bubble wrap.

D.2 Emissivity

Data were collected with an emissivity of 0.92 set as default on the thermal camera instrument, unbeknownst to me. This was later corrected during data processing, so that radiative heat fluxes were calculated with an emissivity of 1.0. Thus, it is assumed that the lava lakes' surfaces behave as blackbodies. Emissivity is not known for phonolite in the short-wave infrared, however authors have often assumed blackbody behavior due to lack of widely-accepted values for emissivity (Pieri et al., 1990; Oppenheimer and Yirgu, 2002; Oppenheimer et al., 2004; Harris et al., 2005).

D.3 Data Processing

Raw data image files are converted via Thermacam Researcher software to MatLab format on a folder by folder basis. Then, in Interactive Data Language (IDL) software, the MatLab files are converted to ENVI (Environment for Visualizing Images) format

and timing data files via an IDL script written for the purpose. A second IDL script is then applied to select the lava lake pixels out of the entire image and process the lava lake pixel temperature values through the Stefan-Boltzmann law, resulting in the total radiative heat flux (Q_{rad}) for the image.

D.4 Processing Parameters

D.4.1 Mid-range filter datasets

Thresholding was used to choose the lava lake pixels from the image. If a pixel temperature was greater than 250°C, it was included in the radiance calculation. Threshold parameters were checked and selected by viewing the thermal images in ENVI, to ensure that all lava lake pixels and only lava lake pixels were included in the radiative heat calculation. Saturated pixels, those with temperatures greater than 800°C (1073K), were not automatically included in the radiance calculation and hence, had to be added manually. Saturated pixels (0-366) were counted for each image and then added to the radiative heat flux by assuming the pixel temperature was 927°C (the maximum temperature recorded for either lava lake surface). Each saturated pixel added ~0.11MW to the total radiative heat flux for a given image, causing an increase in the average daily radiative heat flux of up to 2%.

D.4.2 High-range filter datasets

There are 3 sets of high-range filter data: one of the Main lava lake and two of Werner's lava lake. High-range filter dataset processing required a slightly different treatment. Because of the filter range (~600-1500°C), pixels with temperatures below ~483°C could not be resolved from the background, during processing (Fig. D1). Therefore only pixels with temperatures greater than 483°C are included in the

analysis, which amounts to approximately half of the area of the lake. High-range filter datasets are not useful for calculating radiative heat fluxes. Rather, their use is in observing temporal variations in lava lake surface temperature and resolving the highest temperature pixels of the lava lake surface that saturate in the medium-range filter (Fig. D1).

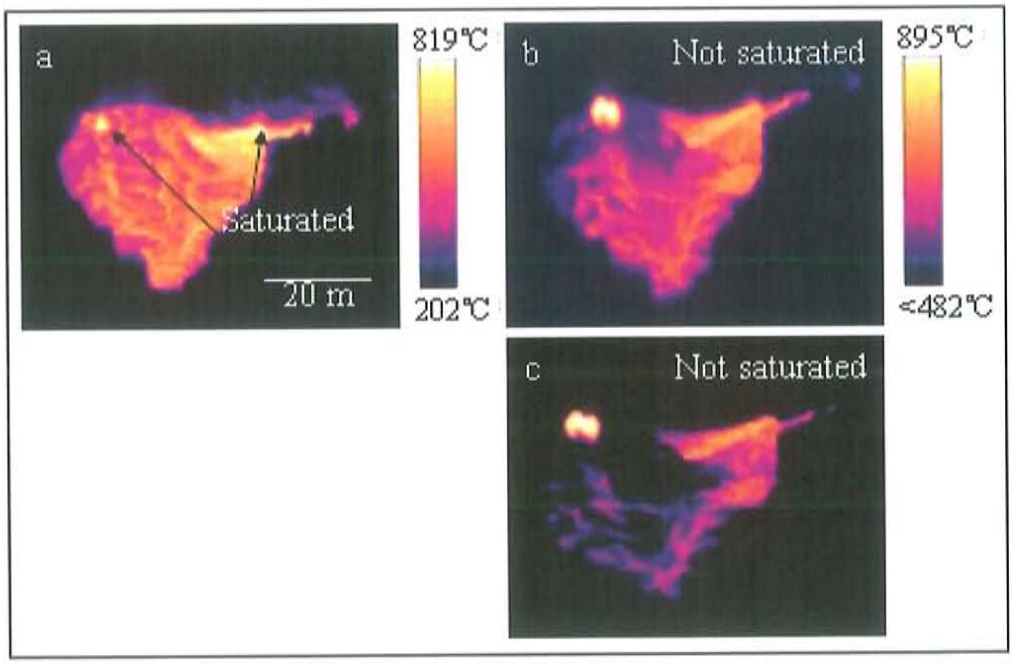

Figure D5. Werner's lava lake observations made on 21 Dec 2004. a) A medium-range filter image with areas of saturation surrounding Strombolian bubble (left arrow) and lava source (right arrow). b) A high-range filter image, adjusted for visibility, showing a Strombolian eruption with no pixels saturated (note higher temperature bar). c) The same high-range filter image showing actual pixels that can be resolved.

Appendix E. Convective Heat Flux from the Lava Lakes

E.1 Introduction

In order to determine the total heat flux from the lava lakes of Mount Erebus volcano and hence, to calculate the magma flux rate, all types of heat must be summed. Heat is transferred in three ways: radiation, convection, and conduction. While the former is the main topic of this research project, appendices E and F are designed to explain the relevant concepts of the latter two heat transfer methods.

E.2 Forced vs. Free Convection

Convection is a specific form of heat transfer which, simply stated, consists of fluid circulation driven by a temperature gradient (Pitts and Sissom, 1991). Convection can either be free or forced. If a fluid is forced by or through a surface that is hotter or colder than the fluid this is forced convection (Pitts and Sissom, 1991). The coils used in cooling a refrigerator, a home heating furnace and wind are common forcing components. Free, or natural, convection is a result of the movement of a fluid (like air) due to density changes that occur during the heating process (Pitts and Sissom, 1991). A prime example of natural convection is the convection current that forms near a large body of water, which serves to cool the land during the day and heat the land during the night, keeping waterside land temperatures moderate.

In this case, the lava lakes are exposed at the bottom of a 200m-deep, steep-sided crater. Certainly, wind does frequently stir the air within the Main Crater; this is evident by observing that the plume rises in different locations around the inside of the Main Crater. However, during thermal observations, weather conditions were

extremely calm and therefore, only free convection heat flux has been calculated for the lava lakes.

E.3 Free Convection Calculation Set-up

The convective heat flux from the Main Lake is modelled as the natural heat loss from a horizontal circular plate of 42m diameter with an average upper surface temperature of 843K to air at 253K. The calculation is performed in two parts; first, the Rayleigh number (Ra) is calculated to determine if air flow is turbulent or laminar:

$Ra_L = [g \beta (T_s - T_\infty) L^3 Pr]/\nu^2$, where L = 0.9x lake diameter = 37.8m. (1)

All parameters (except β) are evaluated at the "film" temperature (T_f),

$T_f = (T_s + T_\infty)/2 = 548K\ (275^\circ C)$ (2)

therefore,

$\nu = 4.434 \times 10^{-5}\ m^2\ s^{-1}$ $k = .04357\ W\ m^{-1}\ K^{-1}$ $Pr = 0.680$

$\beta = 1/T_\infty = 3.95 \times 10^{-3}\ K^{-1}$

The Rayleigh number is 4.3×10^{14} and so, the air flow over the surface of the lava lake is turbulent (Pitts and Sissom, 1991) and the appropriate calculation is then used to determine the total convective heat flux (Q_{conv}).

$Q_{conv} = k\ (0.14)\ (Ra_L)^{1/3}\ (L)(T_s - T_\infty) = 4.1MW$ (3)

The same calculation was completed for Werner's Lake, with an average surface temperature range of 770-870K, and yielded 8 MW convective heat flux. The convective heat fluxes of 4.1 MW and 8 MW are equivalent to roughly one-third of the average radiative heat flux.

Note: In the main text body, this equation has been reduced for simplicity's sake and to facilitate comparison to other models of convective heat calculation. The simplified equation is:

$$Q_{conv} = k\,(0.14)\,[(g\,\beta\,Pr)\,/\nu^2\,]^{1/3}\,(1.8\,r)^2\,(T_s - T_\infty)^{4/3}$$

where r is the radius of the lava lake.

Appendix F: Lava Lake Surface Temperature Corrections

Previous workers have applied corrections to apparent surface temperatures for: solar radiation reflected from the surface of the lava (Flynn et al., 1993), the lava surface emissivity (Salisbury and D'aria, 1994), the viewing angle of the instrument, more specifically the skew and distortion of pixels resulting from the viewing angle, and the absorption of lava lake radiation by gases (Sawyer and Burton, 2006). Solar reflectance from the surface of the lakes was not accounted for in this study because the Antarctic summer sun is only ~15-25° degrees above the horizon at all times and does not shine directly into the Inner Crater during thermal observations. Surface temperatures reported were all calculated for an assumed emissivity of 1.0, approximating blackbody behaviour. The effect of an oblique instrument viewing angle has not been taken into account in this study. The resulting total effect on heat flux determinations has been found to be small, and further minimized by long occupations of changing areas of incandescence (Oppenheimer and Yirgu, 2002).

Temperatures have been corrected for gas-induced decrease in radiative transfer. Path amounts of volcanic and atmospheric gases based on simultaneous measurements obtained, from the same observation location, with an open-path Fourier transform infrared spectrometer (FTIR) have been used to correct a quantity of surface lake temperatures. Figure F1 shows the corrected versus uncorrected temperature in a sample correction procedure; note that correction factor increases with increasing temperature (Sawyer and Burton, 2006). This correction displays the effect of volcanic gas absorption on attenuating the source radiative signal and in this case, resulted in apparent temperatures 30-70C lower than corrected temperatures. Similar

results were determined for both lava lakes. Unless specifically stated, all reported temperatures are uncorrected.

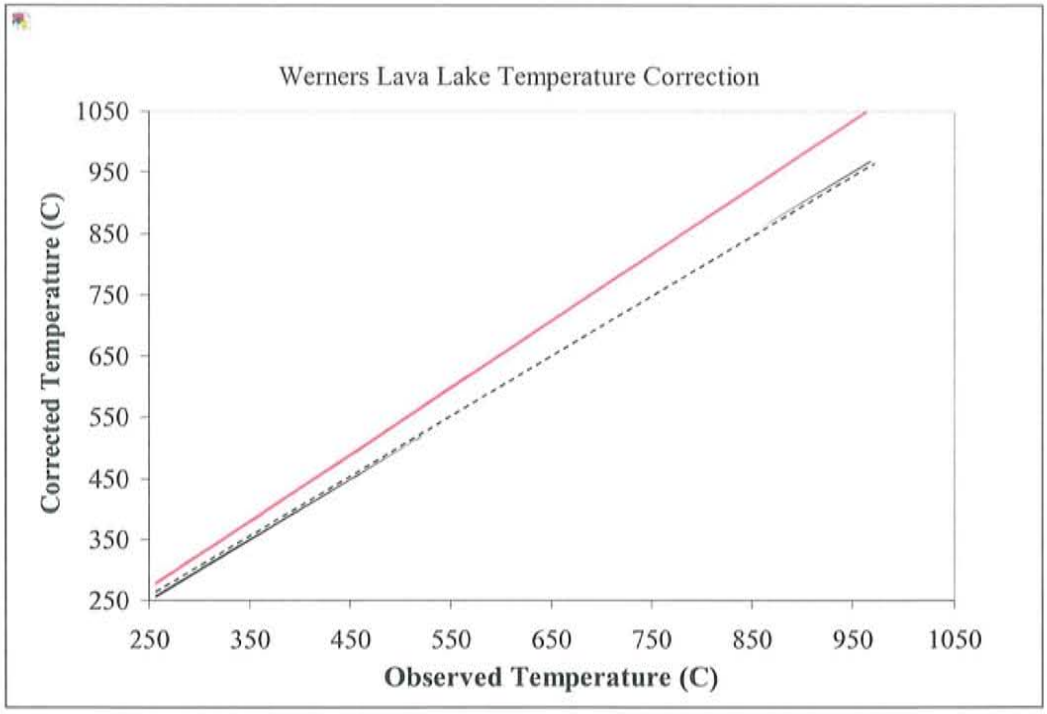

Figure F1. Graph shows corrected surface temperatures on Werners lava lake. The dashed line corresponds to a 1:1 relationship between observed and corrected temperatures. Gas absorption corrections show a 30-70˚C underestimate in observed temperatures.

Acknowledgements

References

Anonymous, 2000. New Book of Popular Science. Electrical Energy, Grolier,

Allard, P., 1997. Endogenous magma degassing and storage at Mount Etna. Geophysical Research Letters, 24 (17): 2219-2222.

Aster, R., Mah, S.,Kyle, P., McIntosh, W., Dunbar, N. Johnson, J., Ruiz, M., and McNamara, S., 2003. Very long period oscillations of Mount Erebus Volcano. Journal of Geophysical Research-Solid Earth, 108 (B11): 2522.

Behrendt, J.C. Duerbaum, H.J.,Damaske, D., Saltus, R., Bosum, W., and Cooper, A.,l., 1991. Extensive volcanism and related tectonism beneath the Ross Sea continental shelf, Antarctica: Interpretation of an aeromagnetic survey. In: M.R.A. Thompson, J.A. Crame and J.W. Thomson (Editors), Geological Evolution of Antarctica. Cambridge University Press, Cambridge, UK, pp. 299-304.

Burgi, P.Y., Caillet, M. and Haefeli, S., 2002. Field temperature measurements at Erta'Ale Lava Lake, Ethiopia. Bulletin of Volcanology, 64 (7): 472-485.

Caldwell, D. and Kyle, P., 1994. Mineralogy and geochemistry of ejectra erupted from Mount Erebus, Antarctica between 1972 and 1986. In: P. Kyle (Editor) Volcanological and Environmental Studies of Mount Erebus, Antarctica. Antarctic Research Series. American Geophysical Union, 147-162.

Clocchiatti, 1976. Bulletin de la Societe Francaise de Mineralogie et de Cristollagraphie, 99 98-110.

Davies, A., Chien, S., Baker, V., Doggett, T., Dohn, J., Greeley, R., Ip, F., Castoo, R., Cichy, B., Rabideau, G., Tran, D., and Sherwood, R., 2005, submitted. Monitoring Active Volcanism with the Autonomous Sciencecraft Experiment (ASE) on EO-1. Remote Sensing of Environment,

Dibble, R., in prep.

Dibble, R., Kyle, P. and Skov, M., 1994. Volcanic activity and seismicity of Mount Erebus, 1986-1994. Antarctic Journal of the United States, 29 11-14.

Dunbar, N., Cashman, K. and Dupre, R., 1994. Crystallization processes of anorthoclase phenocrysts in the Mount Erebus magmatic system: Evidence from crystal composition, crystal size distributions, and volatile content of melt inclusions. In: P. Kyle (Editor) Volcanological and Environmental Studies of Mount Erebus, Antarctic Research Series, vol. 66. American Geophysical Union,

Esser, R., Kyle, P. and McIntosh, W., 2004. 39Ar/40Ar dating of the eruptive history of Mount Erebus Volcano, Antarctica: volcano evolution. Bulletin of Volcanology, 66 671-686.

Evans, B.W. and Moore, J.G., 1968. Mineralogy as a function of depth in the Prehistorical Makaopuhi Tholeiitic lava lake, Hawaii. Contributions in Mineralogy and Petrology, 17 (2): 85-115.

Flynn, L.P., Mouginis-Mark, P.J., Gradie, J.C. and Lucey, P.G., 1993. Radiative temperature-measurements at Kupaianaha Lava Lake, Kilauea Volcano, Hawaii. Journal of Geophysical Research-Solid Earth, 98 (B4): 6461-6476.

Francis, P., Oppenheimer, C. and Stevenson, D., 1993. Endogenous Growth of Persistently Active Volcanoes. Nature, 366 (6455): 554-557.

Giggenbach, W., Kyle, P. and Lyon, G., 1973. Present volcanic activity on Mount Erebus, Ross Island, Antarctica. Geology, 1 135-136.

Glaze, L., Francis, P.W. and Rothery, D.A., 1989. Measuring thermal budgets of active volcanoes by satellite remote-sensing. Nature, 338 (6211): 144-146.

Hardee, H.C., 1980. Solidification in Kilauea-Iki Lava Lake. Journal of Volcanology and Geothermal Research, 7 (3-4): 211-223.

Harris, A., Carniel, R. and Jones, J., 2005. Identification of variable convective regimes at Erta Ale Lava Lake. Journal of Volcanology and Geothermal Research, 142 (3-4): 207-223.

Harris, A.J.L., Butterworth, A.L., Carlton, R.W., Downey, I., Miller, P., NAvarro, P., and Rothery, D.A. 1997. Low-cost volcano surveillance from space: case studies from Etna, Krafla, Cerro Negro, Fogo, Lascar and Erebus. Bulletin of Volcanology, 59 (1): 49-64.

Harris, A.J.L., Flynn, L.P., Rothery, D.A., Oppenheimer, C. and Sherman, S.B., 1999a. Mass flux measurements at active lava lakes: Implications for magma recycling. Journal of Geophysical Research-Solid Earth, 104 (B4): 7117-7136.

Harris, A.J.L. and Stevenson, D., 1997. Magma budgest and steady-state activity of Vulcano and Stromboli. Geophysical Research Letters, 24 (9): 1043-1046.

Harris, A.J.L., Wright, R. and Flynn, L.P., 1999b. Remote monitoring of Mount Erebus volcano, Antarctica, using polar orbiters: Progress and prospects. International Journal of Remote Sensing, 20 (15-16): 3051-3071.

Huppert, H.E. and Hallworth, M.A. 2006. Bi-directional flows in constrained systems, Journal of Fluid Mechanics (in press)

Jaupart, C. and Tait, S., 1995. Dynamics of differentiation in magma reservoirs. Journal of Geophysical Research, 100 (B9): 17615-17636.

Jellinek, A.M. and Kerr, R.C., 2001. Magma dynamics, crystallization, and chemical differentiation of the 1959 Kilauea Iki lava lake, Hawaii, revisited. Journal of Volcanology and Geothermal Research, 110 (3-4): 235-263.

Kazahaya, K., Shinohara, H. and Saito, G., 1994. Excessive degassing of Izo-oshima volcano- magma convection in a conduit. Bulletin of Volcanology, 56 (3): 207-216.

Kyle, P., 1977. Mineralogy and glass chemistry of volcanic ejecta, from Mt. Erebus, Antarctica. New Zealand Journal of Geology and Geophysics, 20 (6): 1123-1146.

Kyle, P., 1979. Volcanic activity of Mount Erebus 1978-1979. Antarctic Journal of the United States, 14 (5): 35-36.

Kyle, P., 1986. Volcanic activity of Mount Erebus 1984-1986. Antarctic Journal of the United States, 21 (5): 7-8.

Kyle, P., 1990a. Erebus Volcanic Province. In: W. LeMasurier et al. (Editors), Volcanoes of the Antarctic Plate and Southern Oceans, Antarctic Research Series, Volume 48. American Geophysical Union,

Kyle, P., 1990b. McMurdo Volcanic Group, western Ross Embayment. In: W. LeMasurier et al. (Editors), Volcanoes of the Antarctic Plate and Southern Oceans, Antarctic Research Series, Volume 48. American Geophysical Union, p. 19-25.

Kyle, P., Dibble, R., Giggenbach, W. and Keys, W.H., 1982. Volcanic activity associated with the anorthoclase phonolite lava lake, Mount Erebus, Antarctica. Antarctic Geoscience, 11 270-271.

Kyle, P. and McIntosh, W., 1978. Volcanic activity of Mt. Erebus 1977/78. Antarctic Journal of the United States, 13 (4): 32-34.

LeMasurier, W., 1990. Late Cenozoic volcanism on the Antarctic plate—an overview. In: W. LeMasurier et al. (Editors), Volcanoes of the Antarctic Plate and Southern Oceans, Antarctic Research Series, Volume 48. American Geophysical Union, 1-17.

Lillesand, T.M. and Kiefer, R.W., 2000. Remote Sensing and Image Interpretation. John Wiley & Sons, Inc., New York, 724p pp.

McClelland, L., Simkin, T., Summers, M., Nielsen, E. and Stein, T., 1989. Global Volcanism 1975-1985. Prentice Hall, 655 pp.

Oppenheimer, C. and Francis, P., 1998. Implications of longeval lava lakes for geomorphological and plutonic processes at Erta 'Ale volcano, Afar. Journal of Volcanology and Geothermal Research, 80 (1-2): 101-111.

Oppenheimer, C. Kyle, P. Tsanev, V., McGonigle, A.J.S., Mather, T., and Sweeney, D. 2005. Mt. Erebus, the largest point source of NO2 in Antarctica. Atmospheric Environment, 39 6000-6006.

Oppenheimer, C., McGonigle, A.J.S., Allard, P., Wooster, M.J. and Tsanev, V., 2004. Sulfur, heat, and magma budget of Erta 'Ale lava lake, Ethiopia. Geology, 32 (6): 509-512.

Oppenheimer, C. and Yirgu, G., 2002. Thermal imaging of an active lava lake: Erta 'Ale volcano, Ethiopia. International Journal of Remote Sensing, 23 (22): 4777-4782.

Pieri, D.C., Glaze, L. and Abrams, M.J., 1990. Thermal radiance of observations of an active lava flow during the June 1984 eruption of Mount Etna. Geology, 18 (10): 1018-1022.

Pitts, D.R. and Sissom, L.E., 1991. 1000 Solved Problems in Heat Transfer. Schaum's Solved Problems Series, McGraw-Hill Inc.,

Reagan, M.K., Volpe, A.M. and Cashman, K.V., 1992. U-238 Series and Th-232-Series Chronology of Phonolite Fractionation at Mount Erebus, Antarctica. Geochimica Et Cosmochimica Acta, 56 (3): 1401-1407.

Ross, J.C., 1847. A Voyage of discovery and research in the Southern and Atlantic regions, during the years 1839-43., John Murray, London,

Ross, M.J., 1982. Ross in the Antarctic: The Voyages of James Clark Ross in Her Majesty's Ships Erebus & Terror 1839-1843. Caedmon,

Rothery, D.A. and Francis, P., 1990. Short wavelength infrared images for volcano monitoring. International Journal of Remote Sensing, 11 (10): 1665-1667.

Rothery, D.A. and Oppenheimer, C., 1994. Monitoring Mount Erebus by satellite remote sensing. In: P. Kyle (Editor) Volcanological and Environmental Studies of Mount Erebus, Antarctic Research Series, vol. 66. American Geophysical Union,

Ruiz, M., 2003. Analysis of Tremor Activity at Mt. Erebus volcano, Antarctica. New Mexico Inst. of Mining and Tech., Socorro.

Salisbury, J.W. and D'aria, D.M., 1994. Emissivity of terrestrial materials in the 3-5um atmospheric window. Remote Sensing of Environment, 47 345-361.

Sawyer, G.M. and Burton, M.R., 2006. Quantification of the radiative effect of volcanic gases on thermal imagery. Geophysical Research Letters, in press

Slezin, Y.B., 2003. The mechanism of volcanic eruptions (a steady state approach). Journal of Volcanology and Geothermal Research, 122 7-50.

Stevenson, D.S. and Blake, S., 1998. Modelling the dynamics and thermodynamics of volcanic degassing. Bulletin of Volcanology, 60 (4): 307-317.

Swanson, D.A., Duffield, W.A., Jackson, D.B., Peterson, D.W.. 1972. The complex filling of Alea crater, Kileauea volcano, Hawaii, Bulletin of Volcanology, 36: 105-126.

Tazieff, H., 1994. Permanent lava lakes- observed facts and induced mechanisms. Journal of Volcanology and Geothermal Research, 63 (1-2): 3-11.

Tilling, R.I., 1987. Fluctuations in Surface Height of Active Lava Lakes During 1972-1974 Mauna Ulu Eruption, Kilauea Volcano, Hawaii. Journal of Geophysical Research-Solid Earth and Planets, 92 (B13): 13721-13730.

Worster, M., Huppert, H.E. and Sparks, R.S.J., 1993. The Crystallization of Lava Lakes. Journal of Geophysical Research, 98 (B9): 15891-15901.

Wright, R., Flynn, L., Garbeil, H., Harris, A. and Pilger, E., 2002. Automated volcanic eruption detection using MODIS. Remote Sensing of Environment, 82 (1): 135-155.

Wright, R. and Flynn, L.P., 2004. Space-based estimate of the volcanic heat flux into the atmosphere during 2001 and 2002. Geology, 32 (3): 189-192.